Spatial structure and variability of the cardiac t-tubular system and its contribution to electrophysiological heterogeneity

Dr. med. Tobias Hannes

Balliol College

University of Oxford

A thesis submitted for the degree of

Master of Science by Research in Clinical Pharmacology

April 2, 2012

Contents

List of Figures

Abstract

Background The cardiomyocyte cell membrane is composed of the surface membrane and a complex system of membrane invaginations, the t-tubules. In keeping with its role in synchronisation of electromechanical coupling, the t-tubular system is distinguished from the cell membrane by its ion channel composition. Variability of the architecture of the t-tubular system might modulate electrophysiological function at the cellular level. Light and electron microscopy-based methods were established to generate three-dimensional models of t-tubular structure. Effects of t-tubular variability on electrophysiological function were investigated using a pseudo-two dimensional model of the ventricular cardiomyocyte. **Methods** Confocal microscopy and electron tomography were used to generate three-dimensional models. Based on the distribution of the t-tubular membrane, electrophysiological parameters were calculated using a mathematical model. **Results and Discussion** Three-dimensional models of t-tubular structure could be generated using different staining protocols for confocal microscopy and different fixation protocols for electron tomography. Advantages and applications of the different methods were discussed. The t-tubular fraction varied considerably among different cardiomyocytes. In the model this gave rise into changes in ionic currents; however variation of t-tubular density lead to heterogeous changes in repolarisation only after simulated inhibition of repolarisation-related membrane currents. **Conclusions** Electron tomography allows generation of structural models at resolution of a few nanometres, however optimisation of fixation protocols is a critical step. Larger volumes can be acquired in living cells with confocal microscopy; however, a large fraction of the t-tubular system is sub-resolution. The variability of the t-tubular system may contribute to electrophysiological heterogeneity in patho-physiologically challenged states, and it forms an interesting target for functional modelling based on three-dimensional models of t-tubular structure.

Word count: 12,650

Chapter 1

Introduction

1.1 T-tubules are a key structure for electromechanical coupling in the heart

1.1.1 The cardiomyocyte as the elementary unit of excitation-contraction coupling in the heart

The coupling of electrical activation to contraction and its fine-tuning is the major function of the heart muscle cell, the cardiomyocyte [12]. Electrical activation manifests in the formation of the action potential. During the action potential, voltage-dependent Ca^{2+}-channels in the cell membrane open. Ca^{2+} is now allowed to enter the cell and binds to ryanodine receptors in the membrane of the sarcoplasmic reticulum, an intracellular membrane system with close juxtapositions to the t-tubular membranes. It acts as the main Ca^{2+}-store in cardiomyocytes. Binding of the relatively small amount of Ca^{2+} that crossed the cell membrane entails the ryanodine receptor to release Ca^{2+} from the sarcoplasmic reticulum. This mechanism has been designated as Ca^{2+}-induced Ca^{2+}-release [35]. The succeeding increase in cytosolic free Ca^{2+}-concentration ($[Ca^{2+}]_i$), promotes the binding of Ca^{2+} to troponin C. The synchronous activation of myosins throughout the cardiomyoyte leads to contraction. As Ca^{2+}-influx *via* voltage-dependent Ca^{2+}-channels and Ca^{2+}-release *via* ryanodine receptors ceases, by inactivation of the respective channels, $[Ca^{2+}]_i$ decreases, largely as a result of the activity of a Ca^{2+}-ATPase in the membrane of the sarcoplasmic reticulum, the so called Sarco-Endoplasmic Reticulum Ca^{2+}-ATPase (SERCA). To decrease the cytosolic Ca^{2+}-concentration and to refill the sarcoplasmic reticulum with Ca^{2+}, a Ca^{2+}-ATPase in the membrane of the sarcoplasmic reticulum, reuptake of Ca^{2+} into the sarcoplasmic reticulum is performed by SERCA. In addition, the Na^{+}-Ca^{2+}-exchanger and a sarcolemmal Ca^{2+}-ATPase extrude Ca^{2+} to the extracel-

lular space and under steady-state conditions this amount is equal to that used for initiation of Ca^{2+}-induced Ca^{2+}-release.

1.1.2 Electrical activation at the cellular level is nearly synchronous

Ca^{2+} is one of the most versatile intracellular messengers. The list of Ca^{2+}-mediated and -modulated cellular processes – besides contraction – seems endless. To name but a few: It is involved in the regulation of numerous ion channels, e. g. in the Ca^{2+}-dependent inactivation of L-type Ca^{2+}-channels, Ca^{2+}-dependent activation of Cl^{-}-channels, in the regulation of K^{+}-channels [1] and in the activation of IP_3-receptors that, in addition to ryanodine receptors, release Ca^{2+} from intracellular stores [38]. It regulates electrical coupling of cardiomyocytes by modification of connexin gating [30]. Gene expression is controlled and modulated by Ca^{2+} [67]. Apoptosis and contracture can result from an inadaequate Ca^{2+}-regulation [37]. In the atrium, it takes part in the regulation of atrial natriuretic peptide secretion [32]. Thus, a spacially and temporally confined control of the Ca^{2+}-concentration is paramount to avoid interference with other cellular functions.
In addition, the spatial control determines also the timing of Ca^{2+}-concentration changes by limiting diffusion pathways to effectors, e. g. ryanodine receptors, and silencers, e. g. SERCA, of the Ca^{2+}-signal. Thus, the dynamics that Troponin C is exposed to that ultimately fine-tune contraction are largely dependent on control of timing and the diffusion distances between the individual components of the contractile apparatus. This is directly evident from the diffusion equation $\frac{\partial C}{\partial t} = D\left(\frac{\partial^2 C}{\partial z^2} + \frac{\partial^2 C}{\partial y^2} + \frac{\partial^2 C}{\partial x^2}\right)$ where C is the Ca^{2+}-concentration and D is the diffusion coefficient.

1.1.3 T-tubules are required for synchronous electromechanical activation of the cells

Ultrastructural aspects of the t-tubular system

Now –in the context of spatial and temporal control of Ca^{2+}-release – t-tubules come into play: with the exception of the perinuclear region, the cardiomyocyte is densely packed with contractile filaments, sarcoplasmic reticulum, and mitochondria. Not that only the distances from the periphery to the center of the cell are relatively far for simple diffusion of Ca^{2+}, all this material itself imposes barriers to diffusion.
Forming a network of invaginations of the cell membrane deep into the cell, t-tubules

are able to deliver action potential related changes in transmembrane potential to the site of excitation-contraction coupling with minimal delay. This leads to nearly synchronous Ca^{2+} release.

T-tubules were first discovered in 1957 in the canine myocardium [61]. The openings of the t-tubules to the extracellular space on the cellular surface were resolved using freeze fracture in 1967 [79]. In 1971, the continuity between t-tubular and interstitial space was demonstrated using colloidal tracers [83]. Three-dimensional structure of cardiac t-tubules was first modelled in 1995 based on electron micrographs of serial thin sections [4] and subsequently in 1999 the structure of a whole rat cardiomycoyte was resolved with confocal microscopy [96].

T-tubules occur every 2 μm adjacent to a Z line which is formed by contractile filaments and form an intracellular interface with the sarcoplasmic reticulum. Their diameters vary between 40 and 450 nm [76]. Depending on species, estimates of the surface fraction of sarcolemma that is part of the t-tubular system range from 21% to 64% in ventricles of the mammalian heart while the contribution to the cell volume – in those calculations t-tubules were regarded as a fraction of the cell although their content is continuous with the extracellular space – ranges from 0.8% to 3.2% [12]. Internalisation of the t-tubular membrane by brief application of the high-osmotic substance formamide leads to a reduction of ≈25% of the cell capacitance [21, 18, 25, 56, 95, 112], a parameter that is obtained by patch clamp measurements and correlates with cell surface area. However, cell capacitance measurements before and after detubulation lead to an underestimation of the t-tubular fraction [18]. Thus, the t-tubular fraction substantially contributes to the surface area of the cell. Besides the part that is transversal to the cell's long axis, axially oriented tubules can be found. The axial fraction depends on species and is highly pronounced in ventricular cardiomyocytes of the rat [9, 12].

Another interesting aspect are the energetics of t-tubules. One can imagine, given the astonishing complexity of the system [96, 86], that maintenance is energetically demanding for the cell. The rate of t-tubule loss during culture after isolation to single cells could be regarded as an indirect measure of this. Within 72 hours, about 50% of t-tubules disappear in rat cardiomyocytes [78]. In addition, metabolic impairment in the course of ischaemic cardiomyopathy leads within days to weeks to a decrease in t-tubular density and loss of regularity [64, 48].

Only mammalian cardimoycytes have so far been reported to be tubulated [12]. However, many mammalian cardiomyocytes have a very sparse t-tubular system or even no t-tubules at all. In rodent atria, the t-tubular system is rudimentary both in

quantity and regularity [10, 42, 51, 14, 95], although in larger animals an extensive t-tubular system can be found in the atria as well [31]. T-tubules appear relatively late during development. In the neonatal period, t-tubules are absent in ventricular cardiomyocytes [109, 88]. In these non-tubulated cells, non-uniform Ca^{2+}-release patterns are observed [47, 50, 95]. This underlines the importance of t-tubules for the synchronisation fo Ca^{2+}-release.

1.2 T-tubules as a specialised membrane system

1.2.1 The t-tubular system is a restricted diffusion space

Potassium diffusion

Potassium is the major regulator of the resting membrane potential. The Nernst potential for potassium is $E_M = \frac{RT}{F} ln \frac{[K^+]_o}{[K^+]_i}$ where R is the universal gas constant, T is the temperature, F is the Faraday constant, K_o^+ is the extracellular and K_i^+ is the intracellular concentration. A typically assumed potassium gradient is $K_i^+ \approx 140$ mM and $K_o^+ \approx 5$ mM resulting in a potassium equilibrium potential of $E_M = -85$ mV.

The main driver of this huge gradient is the Na^+-K^+-ATPase. As the activity of the Na+ -K+ -ATPase is strongly regulated by $[K^+]_o$, small increases in the extracellular potassium concentration have significant effects on the resting membrane potential and thus on cellular excitability.

Alterations in the extracellular potassium concentration primarily change the resting membrane potential and the action potential waveform. In addition, effects on contractility can be observed. However, those depend on cell type and species: while a reduction in the extracellular potassium concentration from 5 to 1 $\frac{\text{mmol}}{\text{L}}$ has a positive inotropic effect in rabbit atrial and rat ventricular cardiomyocytes, contractility increases in rabbit ventricular cardiomyocytes [15]. The effect on contractility seems to be dependent on the relation of changes of the resting membrane potential and action potential duration. While in rabbit atrial and rat ventricular cardiomyocytes the hyperpolarisation-controlled modulation of the Na^+-Ca^{2+}-exchanger dominates, in rabbit ventricular cardiomyocytes the effect of action potential duration on the transmembrane I_{Ca} results in a net gain of intracellular Ca^{2+}.

Based on these observations, t-tubules come into play again. An accumulation of K^+ in the paracellular space was amply documented in the 70's and 80's [26, 52, 53, 27, 71, 65]. In this context, also a slow potassium diffusion in the t-tubular system was

reported [3, 2]. A major finding was that the accumulation of K^+ in the extracellular space was dependent on the beating rate [65].

As potassium diffusion within the t-tubular system can so far not be directly measured, a simulation study to determine the diffusion constant for K^+ between t-tubules and paracellular space [101] was based on a compartmentalised cylinder. The iterative algorithm was run until the change in K^+ converged with the experimental values resulting in a diffusion constant of 85 $\mu m^2/s$, which is about 9 times lower than in water.

However, the tortuous architecture of the t-tubular system alone does not explain the slow diffusion of K^+. In detubulated cardiomyocytes, current changes which indicated changes in $[K^+]_o$ were still slow [101]. A possible explanation could be that K^+ is trapped in caveolae which are small invaginations of the surface membrane not affected by detubulation and by negative charges of the glycocalix on the surface membrane.

The restricted K^+-diffusion in the t-tubular lumen could therefore be involved in the regulation of cellular excitability and could additionally modulate contractility.

Calcium diffusion

Ca^{2+} is the mediator of excitation-contraction coupling. Unlike K^+, changes of $[Ca^{2+}]_o$ directly affect contractility. As the t-tubular membrane is the predominant carrier of transmembrane Ca^{2+}-fluxes, the regulation of t-tubular $[Ca^{2+}]$ is particularly important.

Changes of t-tubular $[Ca^{2+}]$ were adressed with patch-clamp studies and optical methods. Shepherd and McDonough [90] used rapid solution changes while recording peak I_{Ca}. I_{Ca} showed a biphasic response to rapid changes of $[Ca^{2+}]_o$ in guinea pig ventricular cardiomyocytes with a fast and a slow phase, while in rabbit atrial cardiomyocytes lacking t-tubules a slow phase was missing. Assuming that the mean length of t-tubules is approximately 10 μm, Shepherd and McDonough calculated a diffusion constant of 95 $\mu m^2/s$, close to the value Swift *et al.* calculated for K^+ [101]. A comparable observation was made using the membrane-associated Ca^{2+}-indicator Ca^{2+}-Green C18 [13]. After a rapid switch to Ca^{2+}-free solution, a delayed washout of Ca^{2+} out of the t-tubular lumen was observed. In the peripheral regions, washout occured with a $t_{0.5}$ of 0.9 s and in central regions with 1.7 s. When interpreting these results, it has to be kept in mind that the Ca^{2+}-indicator itself acts as a buffer and could contribute to a slower Ca^{2+}-diffusion.

Ca^{2+} therefore can accumulate within the t-tubular system and this accumulation could be involved in the regulation of Ca^{2+}-influx and force generation.

1.2.2 Ion channel distribution in the t-tubular system

Although the t-tubular membrane is continuous with the surface membrane, there is accumulating evidence that the functional properties of both membrane systems are different.

Ca^{2+}-channels. A first hint on a specialisation of the t-tubular membrane was the discovery that the concentration of the L-type Ca^{2+}-channels in isolated membranes is different after fractionation into t-tubular and surface membrane in rabbit, rat, sheep and calf ventricular cardiomyocytes [16, 33]. Furthermore, it was observed that the increase of the L-type Ca^{2+}-channel concentration occurs in parallel to the development of the t-tubular system in the postnatal heart [109, 39]. This correlation holds also true for the decreased L-type Ca^{2+}-channel concentration and t-tubular depletion observed in heart failure. Based on membrane fractionation experiments, Wibo *et al.* [109] estimate a threefold higher concentration in the t-tubular system ($43/\mu m^2$ compared to $13/\mu m^2$), while Doyle *et al.* [33] doubt that precise stochiometries can be given as the membrane fractions were likely to be mutually contaminated. Additionally, the protein localisation can vary depending on a variety of confounding factors, e.g. light. As an example, the Na^+-Ca^{2+}-exchanger can be internalised within hours of light exposure in mice subjected to a light and darkness cycle of 12 hours each [89]. Thus, physiological adaption within short periodical cycles as the rest-and-activity cycle are sufficient to confound measurements of ion channel density. These confounding parameters – if not controlled for – can therefore interfere with the comparability and reproducibility of studies.
Other studies used imaging techniques, mainly immunohistochemistry and thin-section immunogold electron microscopy. Results were, however, contradictory. A comparative study found higher t-tubular immunoreactivity of L-type Ca^{2+} channel subunits in rat, but equal immunoreactivity in rabbit and guinea pig cardiomyocytes compared to the surface membrane [104]. Although immunohistochemical studies are able to resolve differences spatially, a major criticism is that differences cannot be reliably quantified. In addition, the structural differences may not reflect functionality as ion channel gating is largely dependent on the composition of auxiliary subunits and associated proteins.

Although in theory possible by the application of scanning ion conductance microscopy [57], we are not aware of reports on direct current measurements in the t-tubular system as parts of the cell membrane cannot be distinguished by conventional patch clamp techniques. Thus, the major evidence for differences in current densities stems from studies using detubulation by osmotic shock. The brief application of formamide results in the internalisation of – depending on the species – about 80% of the t-tubular membrane [18]. This leads to decoupling with the surface membrane. Based on this experimental principle, currents and dependent parameters can be measured before and after detubulation. In the case of the L-type Ca^{2+}-channel, the respective current is I_{Ca} and dependent parameters are action potential duration and Ca^{2+}-release from the sarcoplasmic reticulum. Consistent with the notion that the L-type Ca^{2+}-channel is concentrated in the t-tubular membrane, a decrease can be found in all three parameters after detubulation [20, 17].

Na^+-Ca^{2+}-exchanger. The removal of the bulk of Ca^{2+}-ions is not dependent on the t-tubular membrane as it is driven by SERCA leading to a reuptake of Ca^{2+} in the sarcoplasmic reticulum. The second most important pathway for Ca^{2+}-removal during relaxation is the Na^+-Ca^{2+}-exchanger [12]. Again using detubulation, the Na^+-Ca^{2+}-exchanger was predominantly located in the t-tubular membrane [29, 112]. This was confirmed by immunohistochemical studies [100].

Sarcolemmal Ca^{2+}-ATPase. A single study investigated the localisation of the sarcolemmal Ca^{2+}-ATPase [25] based on Ca^{2+}-imaging before and after application of carboxyeosin, a sarcolemmal Ca^{2+}-ATPase inhibitor, in control and detubulated cardiomyocytes. A contribution of 6% of the total Ca^{2+}-extrusion after the systolic Ca^{2+}-transient was calculated, that vanishes with detubulation.
Although this contribution seems of minor importance, an important role for the control of diastolic $[Ca^{2+}]_i$ has been suggested [24]. This is based on the observation that the sarcolemmal Ca^{2+}-ATPase is a low velocity, but high affinity pump and therefore extrudes Ca^{2+} even at the low concentrations during diastole. Thus, it can be argued that sarcolemmal Ca^{2+}-ATPase could play an important role in rather in diastolic heart failure which is the inability to adaequately relax. Another important aspect is that a variety of proteins bind to the cytoplasmic loop of the sarcolemmal Ca^{2+}-ATPase including neuronal nitric oxide synthase [110]. If thus, as suggest by Chase and Orchard, the sarcolemmal Ca^{2+}-ATPase is located exclusively within the

t-tubular membrane, the signalling cascades these proteins are involved in are modulated by presence and loss of t-tubules. As the binding to sarcolemmal Ca^{2+}-ATPase decreases the activity of neuronal nitric oxide synthase and nitric oxide modulates Ca^{2+}-release from the sarcoplasmic reticulum, the loss of t-tubules could disinhibit nitric oxide synthase and alter excitation-contraction coupling [60]. These findings suggest that the t-tubular membrane is not only specialised in ion channel activity, but also downstream signalling.

Na^+-K^+-ATPase. The Na^+-K^+-ATPase establishes the electrochemical gradients that are necessary for the electrophysiological function of the heart. It actively moves Na^+ out and K^+ into the cell. In addition, it is essential for the Ca^{2+}-gradient across the cell membrane. Only if the Na^+-K^+-ATPase is operating, the Na^+ gradient can drive the Na^+-Ca^{2+}-exchanger to remove Ca^{2+} from the cytosol – what is called the forward mode of the Na^+-Ca^{2+}-exchanger [12]. Enhancement of the reverse mode is the basis of the action of digitalis that has been used in the therapy of heart failure since William Withering discovered its beneficial effects in 1785. The positive inotropic effect of digitalis glycosides is according to the "pump inhibition hypothesis" mainly mediated by inhibition of the Na^+-K^+-ATPase which increases $[Ca^{2+}]_i$ by reducing the forward mode activity of the Na^+-Ca^{2+}-exchanger [58].
With the predominant t-tubular localisation of Ca^{2+}-transporting proteins and the Na^+-Ca^{2+}-exchanger especially, it is an obvious hypothesis that also the Na^+-K^+-ATPase might be predominantly located in the t-tubular membrane. There is evidence in favour of this hypothesis. Berry *et al.* [11] localised $\approx 70\%$ of the α_2- and $\approx 40\%$ of the α_1-subunit in the t-tubular membrane of murine ventricular cardiomyocytes. With the notion that the α_2-isoform has a predominant role in $[Ca^{2+}]_i$-control while the α_1-isoform is a housekeeper for the K^+-gradient [49] this further supports the hypothesis that the differential distribution of the Na^+-K^+-ATPase contributes to excitation-contraction coupling. This distribution was confirmed in other studies [100] adding the observation that the α_3-isoform could not be localised in the t-tubular system [46]. In addition, detubulation experiments localise the main activity of the Na^+-K^+-ATPase in the t-tubules [29].
The importance of the precise colocalisation of the Na^+-K^+-ATPase and Na^+-Ca^{2+}-exchanger in the t-tubular membrane can be illustrated by the pathophysiology of an inherited disorder of heart rhythm, long QT-syndrome 4 [69]. Long QT syndromes are characterised by a prolonged QT time in the electrocardiogram, familial recurrence of sudden cardiac death [87] and a variety of genetic and iatrogenic causes [6].

One mechanism for the co-distribution is the complex formation of the two proteins with the inositole-trisphosphate receptor and ankyrin B [68]. In ankyrin B knock-out mice, dysfunction of Na^+-K^+-ATPase leads to increased reverse Na^+-Ca^{2+}-exchanger mode. The result is a higher Ca^{2+}-inward current that increases the likelihood of ventricular tachycardias [70].

K^+-currents. Although the t-tubular diffusion has been most extensively studied for K^+ (see 1.2.1), few studies are concerned with the distribution of K^+-currents. A major methodological problem is the great variety of K^+-currents. More than 80 K^+-channel related genes have been identified so far; in the heart both voltage-gated K^+-cuurents as the as the rapidly activating and inactivating transient outward current (I_{to1}), the ultrarapid (I_{Kur}), rapid (I_{Kr}) and slow (I_{Ks}) components of the delayed rectifier current and the inward rectifier current (I_{K1}) and ligand-gated currents, including the adenosine triphosphate-sensitive ($I_{K,ATP}$) and the acetylcholine-activated ($I_{K,ACh}$) currents are each functionally highly important [106].
Immunohistochemically $K_V4.2$, a subunit underlying the transient outward rectifier current I_{to}, was located predominantly in t-tubules [105]. The distribution of a variety of currents was investigated in rat ventricular cardiomyocytes before and after detubulation. As current densities did not change, the transient outward rectifier I_{to}, the delayed rectifier I_K, and the inward rectifier I_{K1} were considered as being uniformly distributed while the steady-state potassium current I_{SS} and – as a control for detubulation – the calcium I_{Ca} were predominantly located in the t-tubules [56].

Stretch-activated currents. Mechanosensitive channels – discovered in the early 80's first in skeletal muscle [43] and later in the myocardium [114] – are a mainstay in the feedback regulation of excitation-contraction coupling [55]. Stretch-activated channels – a subentity of mechanosensitive channels – respond within a milliseconds to changes of cell length. Most stretch-activated channels are cation-nonselective.
Detubulation can abrogate the activation of stretch-activated currents. [34]. This raises the question as to how exactly the spatial organisation of the t-tubular system is altered by whole-cell stretch as explored by electron microscopy [54] and more recently by confocal microscopy [66]. In the reported data, t-tubule length decreases $\approx 10\%$ and volume $\approx 12\%$ at 15% stretch. Thus, the t-tubular membrane could play an important role in mediating stretch responses.

Hormonal modulation of I_{Ca}. Hormonal modulation of heart function is an important principle of physiological adaptation. While cardiac output has to be increased during physical and emotional stress, it can be reduced while the body is resting. This is – in a very simplified conceptualisation – achieved by changing the chronotropy (rate of impulse generation), dromotropy (velocity of cardiac conduction), inotropy (amount of force generated) and lusitropy (velocity of relaxation). Catecholamines, e. g. adrenaline, noradrenaline, dopamine, dobutamine, in general have a positive effect on these parameters. Inotropy is regulated, amongst others, by α_1-adrenoceptor-mediated phosphorylation of protein kinase A which leads by modulation of the L-type Ca^{2+}-channel to an increase of I_{Ca}. Thus, the α_1-adrenoceptor predominantly in the t-tubular membrane. Although this aspect has not been investigated in great detail, this hypothesis can be supported by at least a single study [73].

Coupling between the surface and the t-tubular membrane. The synchronous electrical activation of the t-tubular system requires an adaequate coupling between the surface and the t-tubular membrane. As the coupling between both membranes cannot be directly measured, assertions can be made that require the assumption of good coupling as a necessary condition. First, the synchronous activation leads to a synchronous Ca^{2+}-induced Ca^{2+}-release throughout the cell. This is well documented and supported by the observation that a disrupted or missing t-tubular system leads to asynchronicity [18, 47, 95, 113, 63, 97]. Secondly, the action potential is uniform in both membrane systems. If the coupling would be impaired, the differential distribution of ionic currents would lead to a longer action potential in the t-tubules. This is suggested by the finding that formamide-treatment shortens the action potential in tubulated [21, 84], but not in non-tubulated cells [18] and is coherent with simulations based on a biophysical model incorporating a t-tubular compartment [74, 77]. Direct experimental evidence that this is indeed the case comes from the observation that repolarisation throughout the the cell is uniform [23]. Third, it can be expected that decay of subthreshold voltage clamp steps would be monoexponential [85]. If coupling between the surface and the t-tubular membrane was impaired, a biexponential would have to be expected with a first component resulting from the surface and a second resulting from the t-tubular membrane.

1.3 Heterogeneity of cardiomyocyte repolarisation

1.3.1 Is there a connection between t-tubular architecture and repolarisation?

The connection between the topic of the former section – the specialisation of the t-tubular membrane – and the following is not obvious and requires the anticipation of one of the hypotheses: variability of the distribution of t-tubular membrane between ventricular cardiomyocytes could be sufficient to alter electrophysiological function and repolarisation in particular. If this variability exists, the distribution of the predominantly t-tubular currents might be altered as well. Thus, this section introduces the concept of dispersion of repolarisation before the complete hypotheses are formulated.

1.3.2 Role of repolarisation dispersion in the heart

Differences in the electrophysiological function of cardiomyocytes within a specific compartment, e. g. the left ventricle, have long been recognised as a normal feature of the heart. These differences, however, can contribute to disturbances of heart rhythm. Heterogeneity can be found with nearly every aspect of electrophysiological function, yet differences in repolarisation patterns have a distinct role in the theory of the electrocardiogram and heart rhythm disorders.

Repolarisation can be defined as the return of the excited cardiomyocyte to its resting membrane potential. Differences in the duration of the repolarisation have long been recognised [45], however the concept of transmural dispersion of repolarisation has greatly stimulated research, although its significance in human physiology is still highly debated [72]. Although heterogeneity in the heart is recognised in many dimensionalities of the heart, e. g. apex to base, we illustrate the principle of electrophysiological heterogeneity by the concept of dispersion of repolarisation in order to keep conciseness. Its basic assumption is that repolarisation behaviour changes across the ventricular wall from the outside – the epicardium – to the inside of the heart – the endocardium. Within the wall – transmurally – there are different populations of cells. While the epi- and endocardial cells repolarise relatively fast, a third population – the so called M cell – stands out by its long action potential duration [91]. It has been suggested that M cells, although they depolarise before epicardial cells, they are the latest to repolarise because of their long action potential duration. The hallmark feature of M cells is, however, that they prolong their action potential duration unproportionately compared to epi- and endocardial cells in response to slowing of the

heart rate, pharmacological agents and ion channel mutations that prolong the action potential duration.

The concept of transmural dispersion of repolarisation elegantly explains repolarisation waveform in the electrocardiogram – the T wave – [111, 5] as well as the pathophysiology of a variety of rhythm disorders that are characterised by alterations of the T wave [6]. Among those are inherited cardiac rhythm disorders like the long QT syndrome [87], the short QT syndrome [44], the Brugada syndrome [22] as well as pharmacologically induced changes of the electrocardiogram waveform[7].

At the peak of the T wave, the M cells are still depolarised while the epi- and endocardial cells are fully repolarised. The T wave reaches its end when the M cells finish repolarisation. While the existence of M cells and transmural dispersion of repolarisation is excellently documented in the canine heart [8], there are considerable doubts that these phenomena occur in other species. Although positive reports exist for guinea pig [93], humans [59, 41] and pig [99], others could not find evidence for the existence of M cells in the very same species [82]. In addition, there is considerable doubt that, even if M cells existed, they would play a role in the intact heart [103, 102].

1.3.3 Differential ion channel distribution is a basis of eelctrophysiological heterogeneity in the heart

While the rapid depolarisation is carried by an inward movement of Na^+-ions *via* voltage-activated sodium current, the repolarisation is determined by a complex interplay of K^+-, Na^+- and Ca^+-currents. In the canine heart, differences in the cell membrane's permeability for all three ions account for the transmural dispersion of repolarisation as the Na^+-Ca^{2+}-exchanger, [116], the late Na^+-current [115] and the slow component of the delayed rectifier I_{Ks} [62] are differently regulated.

In addition, a variety of other currents are involved in different diseases that are presumably associated with an increased dispersion of repolarisation: a gain-of-function of the L-type Ca^{2+}-current [98, 94] and of the late Na^+-current as well as a loss-of-function of the rapid component of the delayed rectifier and the inward rectifier.

1.4 Aims

Firstly, this thesis presents methods to reconstruct three-dimensional structure of the t-tubular system based on light and electron microscopy. Secondly, based on the specialised membrane properties of the t-tubular system, it can be hypothesised that

variations in the structure might contribute to electrophysiological heterogeneity. We quantified variation of the density of the t-tubular within and between ventricular cardiomyocytes with confocal microscopy and, using a computational model of a ventricular cardiomyocyte incorporating a t-tubular compartment, we explored potential impacts of t-tubular variation on repolarisation.

Chapter 2

Materials and Methods

2.1 Experimental procedures

2.1.1 Solutions

Solution compounds were obtained from Sigma-Aldrich, St. Louis, MO, USA (`www.sigma-aldrich.com`).
Phosphate buffered solution: NaCl 137 $\frac{\text{mmol}}{\text{L}}$, KCl 2.7 $\frac{\text{mmol}}{\text{L}}$, Na_2HPO_4 10 $\frac{\text{mmol}}{\text{L}}$, KH_2PO_4 1.76 $\frac{\text{mmol}}{\text{L}}$, pH 7.4
Tyrode's solution: NaCl 140.0 $\frac{\text{mmol}}{\text{L}}$, KCl 5.4 $\frac{\text{mmol}}{\text{L}}$, $CaCl_2$ $\frac{\text{mmol}}{\text{l.8}}$, if not otherwise stated, $MgCl_2$ 1.0 $\frac{\text{mmol}}{\text{L}}$, HEPES 5 $\frac{\text{mmol}}{\text{L}}$, glucose 11 $\frac{\text{mmol}}{\text{L}}$, pH 7.4
Modified Tyrode's solution: NaCl 128.0 $\frac{\text{mmol}}{\text{L}}$, KCl 2.6 $\frac{\text{mmol}}{\text{L}}$, $CaCl_2$ $\frac{\text{mmol}}{\text{L}}$, $MgSO_4$ 1.18 $\frac{\text{mmol}}{\text{L}}$, KH_2PO_4 1.18 $\frac{\text{mmol}}{\text{L}}$, HEPES 10 $\frac{\text{mmol}}{\text{L}}$, taurine 20 $\frac{\text{mmol}}{\text{L}}$, glucose 11 $\frac{\text{mmol}}{\text{L}}$, pH 7.0

2.1.2 Cell isolation

For confocal microscopy, ventricular cardiomycytes were kindly provided by Philipp Cobden, Department of Physiology, Anatomy and Genetics and for electron tomography by Andy Edwards, Cardiac Physiology Laboratory, University of Colorado at Boulder. Sprague-Dawley rats were killed by cervical dislocation in accordance with Schedule 1 of the UK Home Office Animals (Scientific Procedures) Act of 1987. The heart was excised, transferred into Tyrode's solution containing heparin and Langendorff perfusion was initated. For this, a cannula was inserted retrogradely into the ascending aorta and kept in position by a sutured banding. The cannula was connected to a pump to maintain perfusion controlled by constant flow. Initially, the hearts were perfused with modified Tyrode's solution supplemented with 5,000 $\frac{\text{U}}{\text{L}}$ heparin and subsequently with modified Tyrode's solution with 20.0 $\frac{\text{mmol}}{\text{L}}$ K^+ in exchange for Na^+ to induce cardioplegic arrest. Upon induction of arrest, the perfusate

was changed for 12 min to enzyme-containing solution (high K^+ modified Tyrode's solution supplemented with 0.24 $\frac{\text{mg}}{\text{mL}}$ BlendZymes III, Roche). The predigested ventricular tissue was then harvested to mince it using a sharp pair of scissors in 10 mL of the enzymatic solution. This solution was collected every 5 min (5 repeats), filtered, and centrifuged for 1 min at 18 g (Precision Durafuge 100). The supernatant was discarded, and the cell pellet was resuspended.
For a single experimental day, rabbit instead of rat ventricular cardiomyocytes were obtained from Philipp Cobden, Department of Physiology, Anatomy and Genetics.

2.1.3 Confocal microscopy

Staining

After isolation, cardiomoyocytes were diluted in Ca^{2+}-free Tyrode's solution in order to achieve a cell density of less than 10 cells at 100 times magnification after attachment on coverslips. Coverslips were incubated with a drop of 0.5% poly-L-lysine for 30 min to improve attachment of cardiomyocytes. Coverslips were washed $3x5$ min with Tyrode's solution before 200 μl of cardiomyocyte solution was distributed in the lysin-coated area. Cardiomyocytes were allowed to settle for 15-30 min resulting in microscopically controlled firm attachment controlled by gentle movement of coverslips. Depending on the dye, different staining protocols were used.

Wheat germ agglutinin-Alexa 555. Before cardiomyocytes were placed on the coverslips, wheat germ agglutinin-Alexa 555 (WGA-Alexa 555, Molecular Probes, 5 $\frac{\mu\text{g}}{\text{L}}$, stock solution 5 $\frac{\text{mg}}{\text{mL}}$ dissolved in phosphate buffered solution) was added to the cardiomyocyte solution. Cardiomyocytes were transferred with the dye-containing solution onto the coverslips resulting in simultaneous attachment and staining. After 30 min of incubation with the dye, the solution was replaced with dye-free, Ca^2+-free Tyrode's solution.

Dextran-conjugated dyes. Three different dextran-conjugated dyes were tested differing in mean molecular weight of the conjugated dextran, electrical charge and conjugated dye: 70 kDa with fluorescein (negative net charge), 10 kDa with fluorescein (negative net charge) and 3 kDa with TexasRed (neutral net charge), all purchased from Molecular Probes, each at 0.5, 1, 1.5 and 2 $\frac{\text{mmol}}{\text{L}}$). Cardiomyocytes were incubated with dextran-conjugated dyes with varying incubation times to observe the distribution of the dyes in the t-tubules at different time points. Different concentrations were tested for each dye.

Image acquisition

Cardiomyocytes were imaged using a Leica TCS NT confocal microscope with a 100x objective, numerical aperture 1.4 with the company's software. For later three-dimensional modelling, z-stacks were acquired starting directly above the coverslip and ending ≈ 10 μm. The number of optical sections was calculated with the Leica software.
In addition, fluorescent beads with diameters of 100 nm were imaged to determine the point spread function of the microscope. They were diluted in heated Tyrode's solution with 2% agarose. The solution was transferred onto coverslips and cooled down to avoid Brownian movement of the fluorescent beads during imaging. ≈ 10 z-stackes were acquired of 20 fluorescent beads.

2.1.4 Electron tomography

Fixation

Cardiomyocytes were fixed either using conventional chemical fixation or high-pressure freezing and subsequent freeze substitution. Both procedures were kindly demonstrated by Mary Morphew, Department of Molecular, Cellular and Developmental Biology, University of Colorado at Boulder. For conventional chemical fixation, cells were fixed in phosphate buffered solution containing 2% glutaraldehyde for 40 min and postfixed in 1% OsO4 for 10 min, After dehydration in acetone and embedding in Epon-Araldite resin (Electron Microscopy Sciences, Hatfield, PA, USA), specimens were sectioned with an ultramicrotome (Leica EM UC, Wetzlar, Germany) at a thickness of 250 nm and then transferred onto grids. Gold particles (British Biocell, Cardiff, UK; diameter 15 nm) were added to both surfaces serving as fiducial markers in the following tomogram reconstruction. For high-pressure freezing and subsequent freeze substitution, cardiomyocytes were seeded onto sapphire disks that were coated with poly-D-lysine. After 30 min, cells were washed and incubated with a medium containing 30% dextran (20 kDa, Sigma-Aldrich). Introduced into a specimen carrier, the sapphire disks were transferred into a high-pressure freezer (BAL-TEC HPM 010, BAL-TEC AG, Liechtenstein, now Leica Microsystems). Sapphire disks were kept in liquid nitrogen after freezing and transferred into a freeze substitution system (Leica AFS2, Leica Microsystems). The substitute was composed of anhydrous acetone containing 0.1% dehydrated glutaraldehyde, 0.25% uranyl acetate, and 0.01% osmium tetroxide. Substitution was initiated at -90°C. After 36 hours, temperature was increased to -45°C at a rate of 10°C/h. At -45°C, the specimen was infiltrated with

plastic, UV polymerisation was started. After 45 hours, temperature was increased to room temperature under continuous UV illumination at a rate of 10°C per hour. After freeze substitution and embedding, semithick sections were cut serially using a Leica Ultracut UCT microtome (Leica Microsystems). Sections were collected on Formvar-coated, palladium-copper slot grids and post- stained with 2% UA in 70% methanol, followed by Reynolds lead citrate.

Image acquisition

Slot grids were transferred into a motorised specimen holder which was inserted into a Tecnai TF30 microscope operating at 300 kV (FEI company, Eindhoven, Netherlands).
Image acquisition was controlled with SerialEM (http://bio3d.colorado.edu/SerialEM). Projections were acquired starting at -60° up to +60° with 1° increments. After 121 projections were acquired, specimens were turned by 90° in the x-y-plane and a second series of 121 projections was taken.

2.2 Generation of three-dimensional models

2.2.1 Confocal microscopy

Preprocessing. The model generation was based on two different algorithms for image preprocessing. The first algorithm was designed to optimise the images for later segmentation while retaining as much of the structural information as possible. The second algorithm lead to an additional image stack with the aim to get a first rough segmentation associated with a loss of structural information. The resulting image stack was used as a basis of the latter segmentation to reduce user interaction and computational time.
First of all, images were deconvolved using an iterative Lucy-Richardson algorithm based on the point spread function that was already implemented in Matlab, Image Processing Toolbox. After deconvolution, histogram equalisation was used. For the presegmentated image stack, a global threshold was calculated for each individual image using Otsu's method and, based on the threshold, was converted to a binary image. This was done sequentially for each image of a stack.

Segmentation. Image stacks were loaded into Seg3D (`http://www.sci.utah.edu/download/seg3d/` and – with the information on voxel sizes – exported in the nrrd format. The volumes with preserved structural information were then imported into

ITK-SNAP (`http://www.itksnap.org`) to use the segmentation algorithm based on region growing. The respective presegmented volume was then used to define starting points of the segmentation. The region growing was reiterated until the segmented volume did not change by optical inspection. Now seeds were placed into t-tubules that were missed by the presegmentation and the algorithm was restarted again until detailed optical inspection revealed a good match between segmentation and the raw volume data.

2.2.2 Electron tomography

Generation of tomograms. Tomograms were generated using eTomo, part of the IMOD package (`http://bio3d.colorado.edu/IMOD`). Before a model of the fiducial markers was generated, projections were coarsely aligned by cross-correlation. Then, in a single projections, about twenty to forty fiducial markers were selected. Starting with those seed fiducial positions, eTomo tracked the selected fiducial markers in all projections. If fiducial markers could not be automatically tracked in adjacent projections, they were manually selected. After the set of fiducial coordinates was complete, fiducial coordinates with a high residual error were visually inspected and manually corrected until a mean residual error of less than 0.25 was achieved. With the model of fiducial markers, the projection data was transformed and three small reconstructions were calculated. The borders in the z-axis were drawn by hand in the three reconstructions. With the fiducial marker model and the border model, the final tomogram was calculated.

Segmentation. Sarcoplasmic reticular, t-tubular and mitochondrial membranes were manually traced using IMOD (http://bio3d.colorado.edu/IMOD). To ease segmentation, tracing was started in a x-y-slice. With the tracking tool, shapes were transferred into an adjacent section and corrected using the sculpt function.

2.3 Analysis of variability

As a first approximation of variability, the fraction of the t-tubular system was calculated in two-dimensional images acquired with confocal microscopy of cardiomyocytes stained with WGA-Alexa 555. As this conjugate binds to the glycocalix of the cell membrane, the signal was regarded as representing the t-tubular content. For the comparison of intercell-variability of the t-tubular system, images at 4-6 μm inside of the cell (measured as distance to coverslip) were loaded into MATLAB 7.11.0

(http://www.mathworks.com). A region of interest outside of the perinuclear region of approximately 128x128 pixels was selected. Regions of interest were preprocessed in Matlab using deconvolution and adapted histogram equalisation. After thresholding at 30% intensity as previously done by [31] and removal of groups of less than 20 pixels, pixels above the threshold were considered to belong to the t-tubular system. The sum of positive pixels was divided by the sum of total pixels to obtain the t-tubular fraction. To test for the intracellular variability, the same procedure was done in at least 5 consecutive images of the same cardiomyocyte with a distance of 10 optical sections between each. The t-tubular fractions were compared using MATLAB.

2.4 Functional modelling

To test the impact of t-tubular variability on the electrophysiological function of cardiomyocytes, a model of the guinea-pig ventricular cardiomyocyte by Pásek *et al.* [77] was obtained from the CellML model repository (`http://models.cellml.org/exposure/635e4736ed9c650fb8c8746e9cc229c3`). The unique characteristic of this model is the incorporation of a t-tubular compartment that is separated from the bulk extracellular space by restricted diffusion. According to the differential distribution between cell surface and t-tubular membrane (see Introduction), ionic current densities of the whole cell are expressed as the sum of the t-tubular and cell surface membrane current density. The t-tubular and the surface membranes are parallel connected. The interface between SR and t-tubular membrane – the subspace – is separated from the bulk intracellular space by restricted diffusion. The detailed mathematical formulation of the model can be found in [77].
Simulations were done in OpenCell V 0.8 (`http://www.cellml.org/tools/opencell`) built from source and run with Ubuntu 10.10. Maximum step size was set to 1 ms and point density$_{max}$ to 10^5. The t-tubular volume was varied according to the minimum, 25% percentile, 75% percentile and maximum of the distribution of t-tubular fractions ($F_{T,min}$, $F_{T,p25}$, $F_{T,p75}$ and $F_{T,max}$, given in percent). This was achieved by changing the parameter ρ_m describing the density of t-tubules in the surface membrane and is proportional to the surface of the t-tubular membrane $S_{m,t} = 4\pi^2 r_t L_t r_c L_c \rho_t$ (r_t: mean radius of t-tubules, L_t mean length of t-tubules, r_c radius of the cell, L_c: length of cell). Data were analysed using MATLAB 7.11.0 ((http://www.mathworks.com) and R 2.12 (`http://www.r-project.org/`).

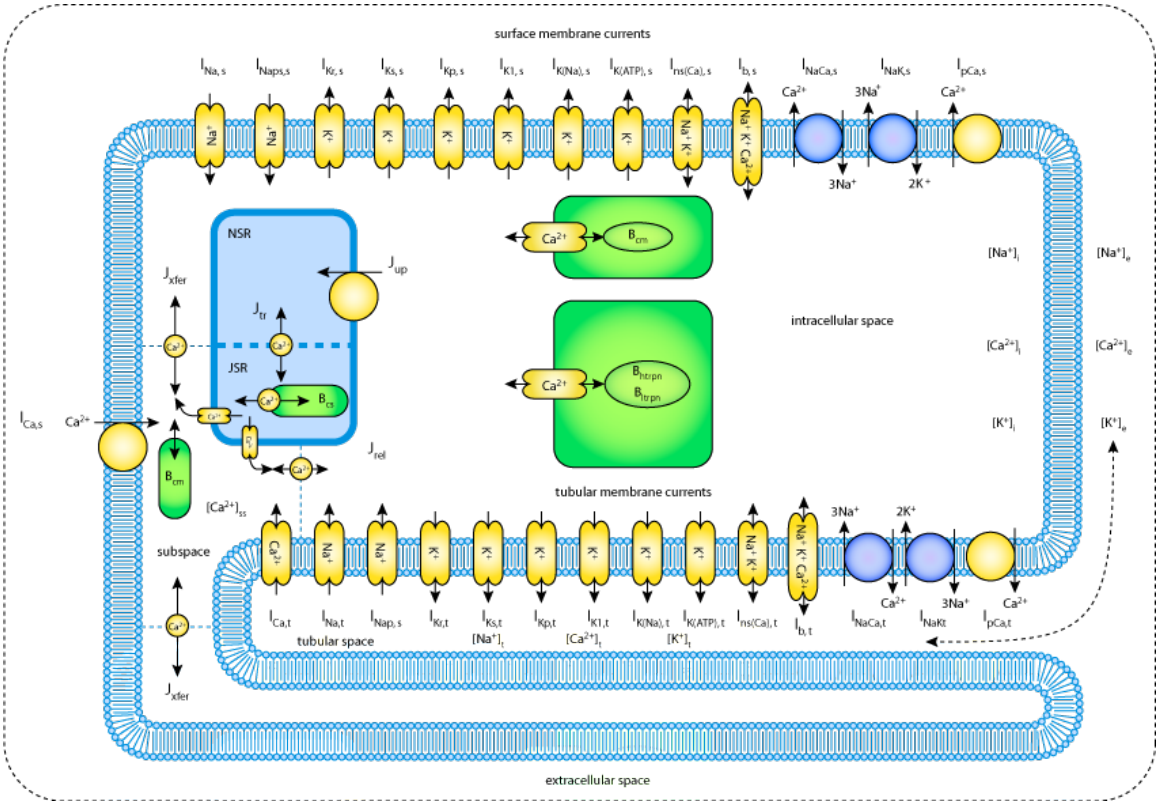

Figure 2.1: Scheme of the model by Pásek *et al.* [77] (CellML model repository). The sarcolemma is represented as a blue bilipid layer, ionic currents as one-arrowed yellow transmembrane symbols, pumps as two-arrowed yellow symbols, exchangers as blue circles, buffers as green squares. The sarcoplasmic reticulum is divided into a junctional (JSR) and a network (NSR) sarcoplasmic reticulum. Rate limited transfer of Ca^{2+} between different intracellular space and subspace is indicated by yellow circles.

Chapter 3

Results

3.1 Two-dimensional representations of the t-tubular system

Staining of the t-tubular system in rat ventricular cardiomyocytes was attempted based on WGA-Alexa 555, a conjugate that binds to the glycocalix of at the outer cell membrane and thus remains inside the t-tubular lumen, and dextran-conjugates with different molecular weights.

While incubation with WGA-Alexa 555 reliably resulted in a t-tubular pattern, the negatively charged dextran-fluorescein conjugate at 70 kDa could be detected in an isolated case and the negatively charged dextran-fluorescein conjugate at 10 kDa could not be detected inside the t-tubular lumen at all. Observation times were increased up to two hours with varying observation intervals. Bath fluorescence was bright in all cases. Observation times were increased up to two hours with varying observation intervals. Experiments with dextran-fluorescein 70 kDa without stimulation were performed at 10 different days with 6 ± 2.1 runs per day. The time course was observed in a single cell. After observation time was completed, dextran diffusion was assessed in at least 10 other cells. Observation times were 15 min in 31 cases, 30 min in 11 cases, 1 hour in 4 cases and 2 hours in 4 cases. For dextran-fluorescein 10 kDa, a mean of 3.2 ± 1.7 runs at 13 experimental days were performed and here, observation times were 15 min in 26 cases, 30 min in 6 cases, 1 hour in 6 cases and 2 hours in 4 cases (see table 3.1).

A facilitation of diffusion by deformation of the t-tubular system has previously been proposed [66, 86]. With the hypothesis that active contraction of the cardiomyocytes could increase uptake of dextran conjugates into the t-tubular system, cardiomyocytes incubated in a Tyrode's solution with Ca^{2+} ($0.9\ \frac{\text{mmol}}{\text{L}}$) were stimulated at different

Dye	n not stimulated	n stimulated
Dextran fluorescein 70 kDa	60 (1)	5 (0)
Dextran fluorescein 10 kDa	42 (0)	4 (0)

Table 3.1: T-tubular prenetration of dextran-conjugates: number of experiments. In brackets: number of experiments with dye detected within the t-tubular system.

frequencies (1-4 Hz) for up to 30 min. This was tried 5 times with dextran-fluorescein 70 kDa and 4 times with dextran-fluorescein 10 kDa. None of the attempts resulted in the detection of dextran-conjugates inside of the t-tubular system.
Therefore, confocal microscopy for three-dimensional modelling and analysis of t-tubular variability were based on WGA-Alexa 555 stainings.

3.2 Three-dimensional representations of the t-tubular system

3.2.1 Confocal microscopy

Image stacks were converted to a volume after deconvolution and adapted histogram equalisation. The region growing algorithm implemented in ITK-SNAP was used for segmentation. Although all parts of the t-tubular system are interconnected *via* the surface membrane, extensive selection of so called seed points within the surface and t-tubular membrane – small cubic or sphaerical volumes wherefrom the segmentation algorithm initiates – was required especially in volumes generated from rat cardiomyocytes, but less so in rabbit cardiomyocytes. This resulted partially from the thinner and more complicated t-tubular system in the rat, but also from an incomplete interconnectivity of the imaged t-tubular system.

To avoid the time-consuming selection of seed points, a presegmented binary image stack was used as a seeding matrix. The preprocessed image stack was further thresholded using Otsu thresholding (see Fig 3.1). Here, a single threshold intensity level is automatically determined and a binary image is generated with zeroes at intensities below and ones at intensities above the threshold intensity. The combined approach reduced user interaction substantially. A representative three-dimensional model is shown in fig. 3.2).
The achieved voxel resolution is anisotropic and was calculated as $0.156\,\mu\text{m} \cdot 0.156\,\mu\text{m} \cdot 0.22\,\mu\text{m}$ (It has to be kept in mind that optical resolution is lower as given in section 2.1.3).

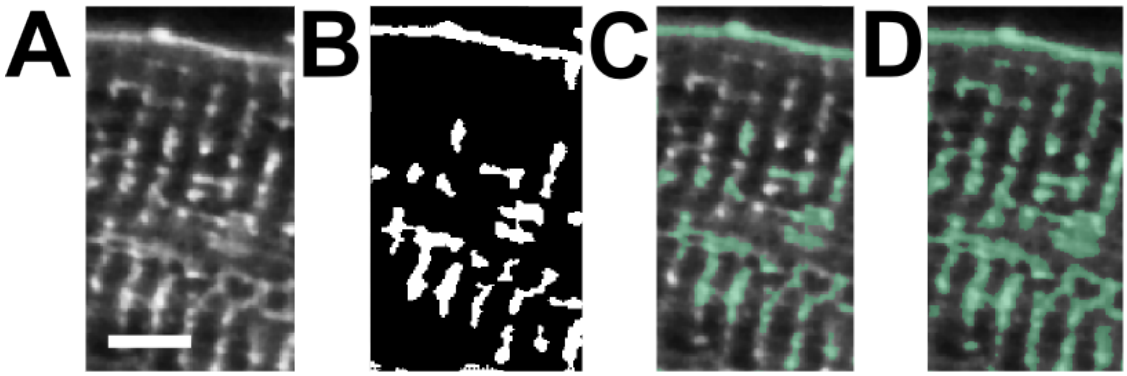

Figure 3.1: Segmentation in confocal volumes (representative slice of a volume) A: Slice after pre-processing, B: Pre-segmentation, white areas represent the pre-segmented membrane, C: Pre-segmentation projected onto slice (green). The pre-segmentation coordinates were used as seed points for region-growing segmentation, D: Region growing after 500 iterations.

3.2.2 Electron tomography

Five datasets were obtained from rat cardiomyocytes; three after chemical fixation and two after high pressure freezing and freeze substitution. Four of the datasets had a mean volume of $2470 \cdot 2470 \cdot 173 \pm 15\text{nm}^3$ with an isotropic pixel spacing of 12.05 Å. The remaining dataset was a $2 \cdot 1$ montage of two adjacent datasets with a total volume of $4703 \cdot 2470 \cdot 205\text{nm}^3$.

For the segmentation, mitochondrial, t-tubular and sarcoplasmic reticular membranes were considered. The membrane configuration was remarkably different after the different fixation protocols. After chemical fixation, especially the outer mitochondrial membrane, but other membranes as well were corrugated (Fig 3.3, B). In addititon, membrane discontinuities could be found after chemical fixation (Fig 3.3, D).

SR membranes could only be detected after chemical fixation (Fig 3.3, B,C), but not after freeze substitution (Fig 3.3, A). The inner mitochondrial membrane was weakly contrasted after freeze substitution; therefore, cristae could only be found after chemical fixation (Fig 3.3, B).

In summary, several ultrastructural details (inner mitochondrial membrane, sarcoplasmic reticulum) were contrasted after chemical fixation, but not after freeze substitution. However, membrane corrugation and discontinuities of membranes were not found after freeze substitution, but not after chemical fixation.

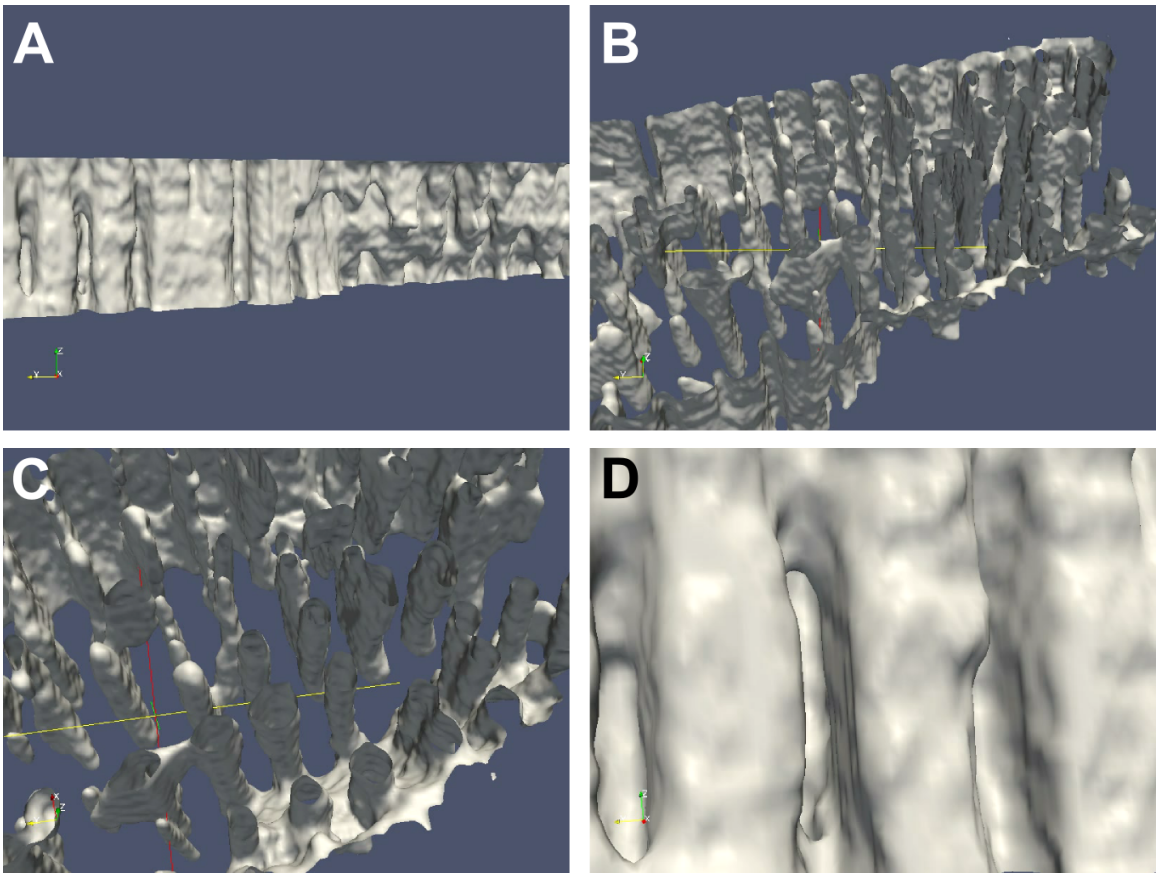

Figure 3.2: Representative three-dimensional model derived from confocal microscopy of a rabbit ventricular cardiomyocyte (Background: blue, sarcolemma: grey, X-axis: red, Y-axis: yellow, Z-axis: green) : A) View at the lateral surface membrane, B) Oblique view into the cell, C) View from top into the cell, D) View at t-tubular mouths of the surface membrane

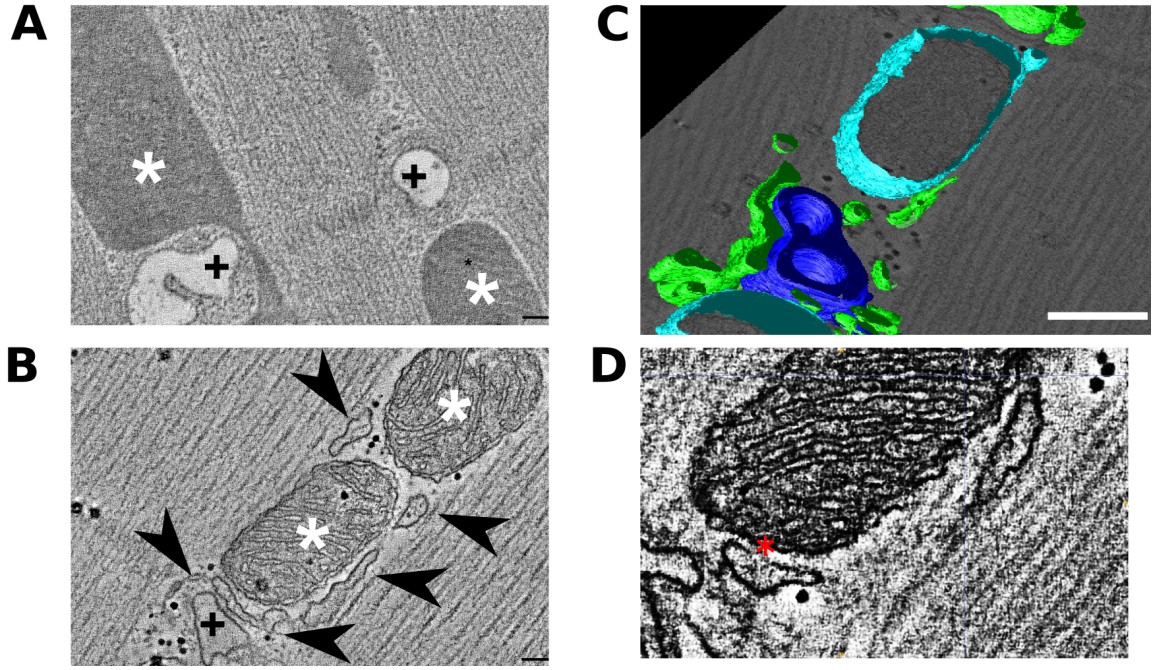

Figure 3.3: Electron tomography of rat ventricular cardiomyocytes. A: After freeze substitution. White asterisks: Mitochondria, black +: t-tubules. Christae within mitochondria are weakly contrasted; a sarcoplasmic reticulum could not be detected. Scale bar: 250 nm. B: After chemical fixation. White asterisks: Mitochondria, black +: t-tubules, black arrowheads: sarcoplasmic reticulum. Scale bar: 250 nm. C: Three-dimensional model projected into a single tomographical slice after chemical fixation. Dark blue: t-tubule, light blue: outer mitochondrial membrane, green: sarcoplasmic reticulum. Scale bar 250 nm. D: Electron tomogram after chemical fixation. Red asterisk: Disconuity in a sarcoplasmic reticulum membrane after chemical fixation

3.3 Structural variability of the t-tubular system

3.3.1 Inter- and intracellular variability

Based on confocal microscopy of cardiomyocytes stained with WGA-Alexa 555, the t-tubular fraction was determined in $N = 54$ different cells as $31.78 \pm 10.78\%$ ranging from 10.53% to 54.13%. 25^{th}, 50^{th}, and 75^{th} percentiles were 26.07%, 32.06% and 38.27%, respectively. To estimate the ratio between between inter- and intracellular variability, the coefficient of variation was calculated as $c_v = \frac{\sigma}{\mu}$ with σ as the standard deviation and μ as the mean of the respective sample population. The variation coefficient for the $N = 54$ different cells was 35.24%. To estimate the intracellular variability, the variation coefficient was calculated in 5 image stacks of 5 different cells based on a mean of 11.8 images (distance 5 optical sections). The coefficient of variation for this population was calculated as $7.91 \pm 2.72\%$, 95% confidence interval 4.09% - 10.26%. The intercellular variability is therefore about between 3.4x to 8.6x higher than the intracellular variability.

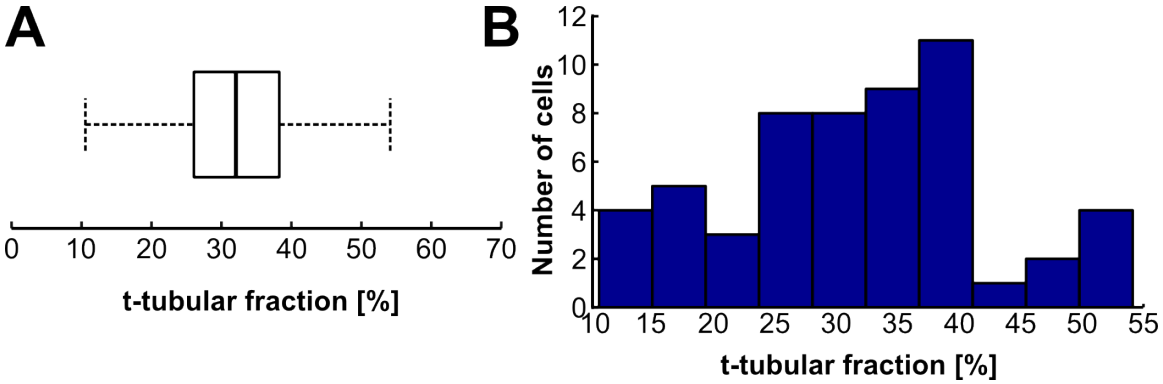

Figure 3.4: Intercellular variability of the t-tubular surface in rat ventricular cardiomyocytes: A) Boxplot, B) Histogram

3.3.2 Modelling of the effects of t-tubular variability on electrophysiology

As variability of the t-tubular density between different cardiomyocytes could be observed (and was higher between cells than within cells), the question whether t-tubular variability has a relevance for cellular electrophysiology was adressed. In the model by Pásek *et al.* [77], the t-tubular system is represented as a cylindric compartment with a surface $S_{m,t} = 4\pi^2 r_t L_t r_c L_c \rho_t$ (r_t: mean radius of t-tubules, L_t mean length of t-tubules, r_c radius of the cell, L_c: length of cell, ρ_t: density of t-tubular ostiae

at the cell surface). ρ_t was multiplied by the minimum, 25$^{\text{th}}$ percentile, mean, 75$^{\text{th}}$ and maximum individually divided by the mean resulting in 5 models at the range of t-tubular densities.

All data were obtained within a cycle of 30 s simulated time after the model was run for 1800 s to achieve steady state.

Effect of t-tubular variability on electrophysiological function under standard conditions

Action potential. Action potential morphology was primarily evaluated by visual inspection (Fig. 3.5, A) and was judged as minimal. Differences were quantified by trapezoidal numerical integration of 30 action potentials at 1 Hz stimulation rate after correcting the offset. F_{Mean} deviated minimally (0.04%) from the mean of the integrals. F_{P25} and F_{P75} deviated 0.62% and -0.74%, respectively. F_{min} was 2.1% greater, F_{max} reduced by 3.26%.

L-type Ca^{2+}-current. The density of t-tubules in the surface membrane positively correlates with the the t-tubular I_{CaL} (Fig. 3.5 C) and, consequently, with the whole cell I_{CaL} (Fig. 3.5) which is the sum of the t-tubular and the surface membrane I_{CaL} ($I_{CaL,c} = I_{CaL,t} + I_{CaL,c}$). Under steady-state conditions, an isolated reduction or increase of $I_{Ca,c}$ leads to an abbreviation or prolongation of the action potential. As depicted in Fig. 3.5 A, the t-tubular density does however not correspond to the action potential duration.
While the t-tubular surface decreases by 33.13% and the whole membrane surface by 31.69% in minimally compared to normally tubulated cardiomyocytes, whole cell I_{CaL} decreases by 35.26%. In maximally tubulated cardiomyocytes the t-tubular surface is 70.33% and the whole membrane surface is 37% larger. Whole-cell I_{CaL} increases by 32.58%.

Ca^{2+}-extrusion. $I_{Ca,P}$, the current of the sarcolemmal Ca^{2+}-ATPase is a pure outward current. Thus the integral corresponds with the amount of Ca^{2+}-ions extruded by the sarcolemmal Ca^{2+}-ATPase. Changes of $I_{Ca,P}$ corresponded with the changes of t-tubular density. At the minimal t-tubular density the whole cell $I_{Ca,P}$ integral was reduced by 36.4%, at the 25$^{\text{th}}$ percentile by 10.1%. At the 75$^{\text{th}}$ percentile an increase by 10.3%, at the maximum by 36.8% could be found. The minimal whole

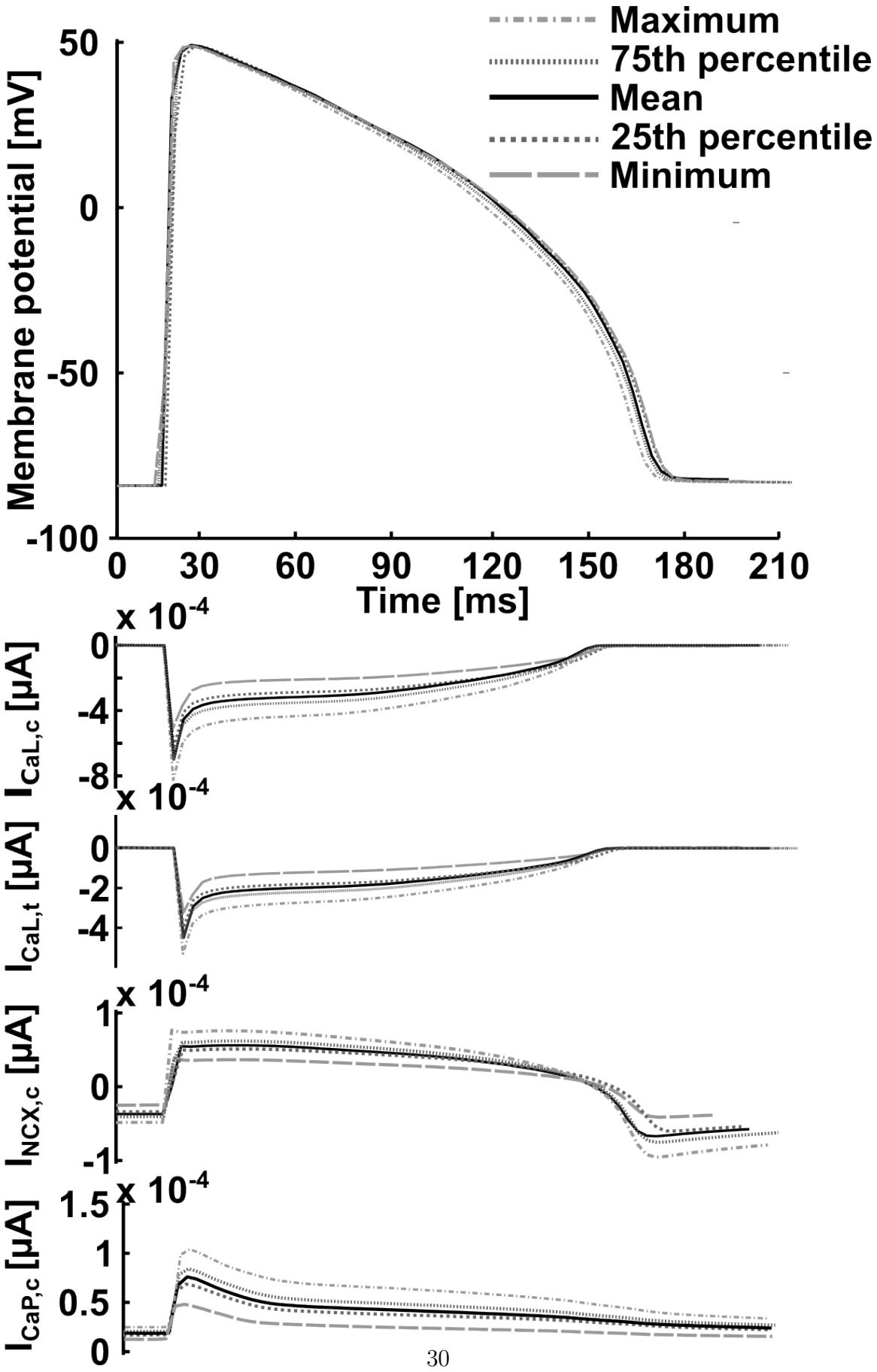

Figure 3.5: Modelling of the action potential duration, whole cell I_{CaL}, t-tubular I_{CaL}, whole cell I_{NCX} and whole cell I_{CaP} at different t-tubular surface densities.

Concentrations	Minimum	P25	Mean	P75	Maximum
$[Ca^{2+}]_{SS}$ $[\frac{\mu mol}{L}]$	0.295	0.326	0.342	0.342	0.374
$[Ca^{2+}]_i$ $[\frac{\mu mol}{L}]$	0.127	0.13	0.131	0.117	0.113
$\mathbf{Ratio}_{i/SS}$	0.43	0.40	0.38	0.34	0.30
$[Ca^{2+}]_t$ $[\frac{mmol}{L}]$	1.74	1.76	1.77	1.77	1.77
$[K^+]_t$ $[\frac{mmol}{L}]$	5.53	5.48	5.48	5.47	5.46
$[Na^+]_t$ $[\frac{mmol}{L}]$	139.97	139.99	139.99	139.99	139.99

Table 3.2: Ion concentrations depending at different t-tubular densities: $[Ca^{2+}]_{SS}$ is the Ca^{2+}-concentration in the subspace, $[Ca^{2+}]_i$ is the Ca^{2+}-concentration in the intracellular space, $[Ca^{2+}]_t$ is the Ca^{2+}-concentration in the tubular space, $[K^+]_t$ and $[Na^+]_t$ are the tubular Na^+- and K^+-concentrations, respectively. P25 and P75 are the 25^{th} and 75^{th} percentile, respectively. All concentrations are given as means in a cycle of 30 stimulated beats at a frequency of 1 Hz.

cell $I_{Ca,P}$ which corresponds to the diastolic activity as well as the peak whole cell $I_{Ca,P}$ showed a similar behaviour.

Ion concentrations. The altered ion channel behaviour may lead to and may also be partially explained by changes in ion concentrations. Table 3.2 summarises the changes depending on the t-tubular densities at the minimum, 25^{th} percentile, mean, 75^{th} percentile and maximum of the empirically determined distribution. While the t-tubular Na^+-concentration changed minimally (0.01% change between minimum and maximum), a small change of the t-tubular K^+(-1.3%) and Ca^{2+}concentration (1.7%) was calculated. The intracellular Ca^{2+}-concentration, however increased with a lower t-tubular density (12.3%), while the Ca^{2+}-concentration in the subspace increased (26.8%). This lead to a decrease in the $\text{ratio}_{i/SS} = \frac{[Ca^{2+}]_i}{[Ca^{2+}]_{SS}}$ (see table 3.2)

Effects of t-tubular density on intracellular Ca^{2+}-cycling. The t-tubular density lead to an opposite behaviour of intracellular and subspace Ca^{2+}-concentrations (Table 3.2). Consequently, a change of the transport of Ca^{2+} between intracellular space, subspace, Ca^{2+}-network and junctional sarcoplasmic reticulum was assumed. The relevant variables are the Ca^{2+}-uptake from the subspace into the Ca^{2+}-network (J_{up}), the transfer between the Ca^{2+}-network and the junctional sarcoplasmic reticulum (J_{tr}), the release from the junctional sarcoplasmic reticulum into the subspace (J_{rel}), the transfer between subspace and intracellular space (J_{xfer}) and finally the Ca^{2+}-leak from the sarcoplasmic reticulum into the intracellular space, which – under steady state conditions – is the difference between J_{rel} and J_{up}. The integrals for an average beat during 30 s stimulation at 1 Hz were calculated using trapezoidal

Variables	Minimum	P25	Mean	P75	Maximum
J_{tr} $x10^{-7}\frac{\text{mmol}}{\text{s}}$	1.23	1.33	1.36	1.40	1.51
J_{rel} $x10^{-7}\frac{\text{mmol}}{\text{s}}$	1.25	1.36	1.45	1.38	1.52
J_{up} $x10^{-7}\frac{\text{mmol}}{\text{s}}$	3.72	3.96	4.02	4.10	4.29
J_{xfer} $x10^{-7}\frac{\text{mmol}}{\text{s}}$	1.66	1.93	2.08	2.08	2.37

Table 3.3: Intracellular Ca^{2+}-cycling: J_{tr}: Transfer between junctional sarcoplasmic reticulum and Ca^{2+}-network, J_{rel}: Ca^{2+}-release from the junctional sarcoplasmic reticulum into the subspace, J_{up}: Ca^{2+}-uptake from the intracellular space into the Ca^{2+}-network, J_{xfer}: transfer between subspace and intracellular space.

numerical integration and are given in table 3.3.
Any of the variables were increased with a higher t-tubular density; this – in addition to higher I_{CaL} – explained the higher mean Ca^{2+}-concentration in the subspace (Table 3.2) despite an equal action potential duration.

Effects of t-tubular density on K^+-currents. Being equally distributed between surface and t-tubular membrane, whole cell (Fig. 3.6 A) and t-tubular (Fig. 3.6 B) I_{Kr} increased with higher t-tubular density and decreased with lower t-tubular density. Whole-cell I_{Kr} increased by 28.38% in maximally and decreased by 34.86% in minimally tubulated cardiomyocytes compared to normally tubulated cardiomyocytes. I_{K1} increases by 36.62% in maximally and decreases by 37.14% in minimally tubulated cardiomyocytes. An 31.6% increase and a 34.86% decrease for I_Ks was observed. Relative to the whole membrane surface, the decrease in minimally tubulated cardiomyocytes was higher than the increase in maximally tubulated cardiomyocytes.

Contribution of t-tubular variability under non-standard conditions

Na^+-K^+-ATPase inhibition. Inhibition of the Na^+-K^+-ATPase was simulated by reduction of the maximal current of the Na^+-K^+-ATPase, I_{NKA}, from 1.5 $\frac{\mu A}{cm^2}$ to 0.5 $\frac{\mu A}{cm^2}$. The action potential was shortened in any of the cases; however shortening was more pronounced in maximally and less pronounced in minimally tubulated cardiomyocytes (Fig. 3.7 A). This could partially be attributed to a steeper reduction of I_{CaL} in maximally tubulated cardiomyocytes during the late repolarisation as indicated by a stronger left-shift of I_{CaL} in fig. 3.7 D than in normally (Fig. 3.7 C) and minimally (Fig. 3.7 B) tubulated cardiomyocytes. Thus, in the case of Na^+-K^+-ATPase inhibition, variability in the degree of tubulation could induce a considerable dispersion of repolarisation.

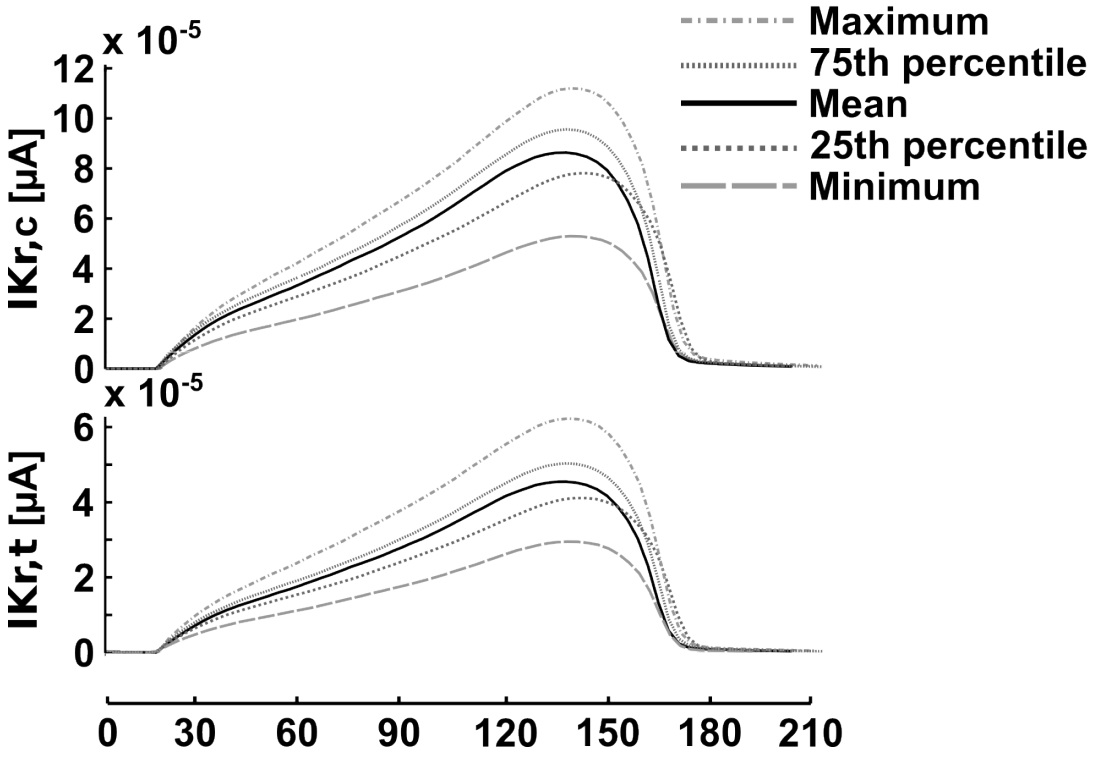

Figure 3.6: Whole cell (A) and t-tubular (B) I_{Kr} during the action potential.

Changes in the extracellular K^+-concentration. The extracellular and t-tubular K^+-concentrations were equally set to 3.5, 5.4 and 7 $\frac{\text{mmol}}{\text{L}}$. These values correspond to the lower limit of reference values in humans (3.5 $\frac{\text{mmol}}{\text{L}}$), the standard model condition which is close to the upper limit of the reference values in humans (5.4 $\frac{\text{mmol}}{\text{L}}$), and a value that corresponds to an elevated plasma concentration (7 $\frac{\text{mmol}}{\text{L}}$), to so called hyperkaliaemia. Fig. 3.8 shows the action potential traces for the maximal, the mean and the minimal t-tubular density. An elevation of the extracellular K^+-concentration lead to a shortening of the action potential, a reduction to a prolongation. While at the standard and the elevated K^+-concentration differences in action potential duration were minimal, a reduction to the lower physiological limit lead to a shortening of the action potential at maximal t-tubular density and a prolongation at minimal t-tubular density. Thus, a low normal K^+-concentration could induce a slight dispersion like the isolated inhibition of the Na^+-K^+-ATPase albeit it prolonged the action potential.

Inhibition of K^+-currents. Among the repolarisation reserve-related currents, I_{Kr}, I_{Ks}, and I_K1 were considered. I_{to}-conductance is set to 0 in the default model conditions and I_{to} was therefore not included. Action potential waveform was uniform

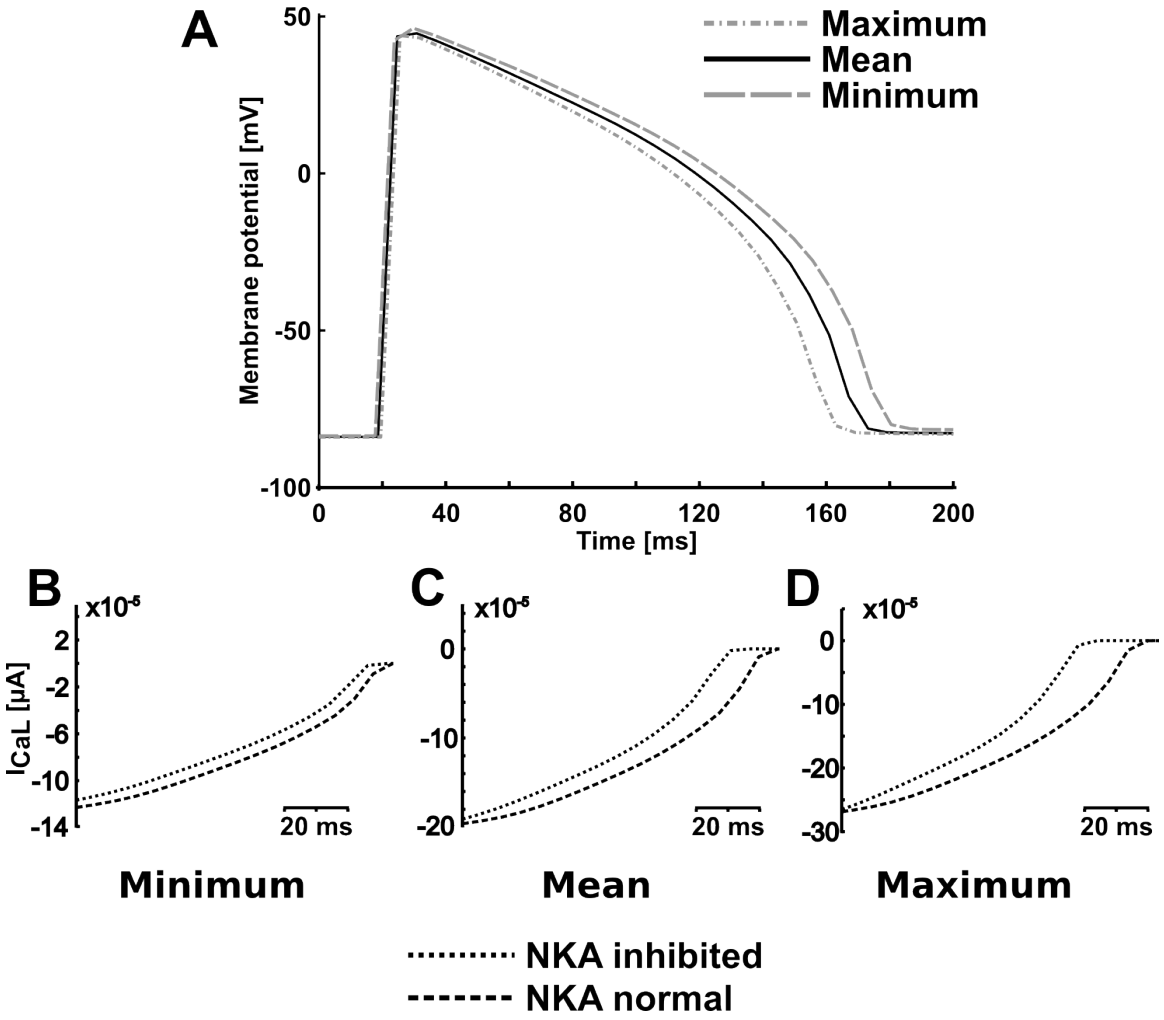

Figure 3.7: Inhibition of the Na^+-K^+-ATPase: A: Shortening of the action potential was less pronounced in minimally tubulated and more pronounced in maximally tubulated cells. B,C,D: Relative reduction of I_{CaL} was highest in maximally tubulated cardiomyocytes (D) and lowest in minimally tubulated cardiomyocytes (B). Mean tubulation fell in between (C). This contributes to the differential shortening of the action potential.

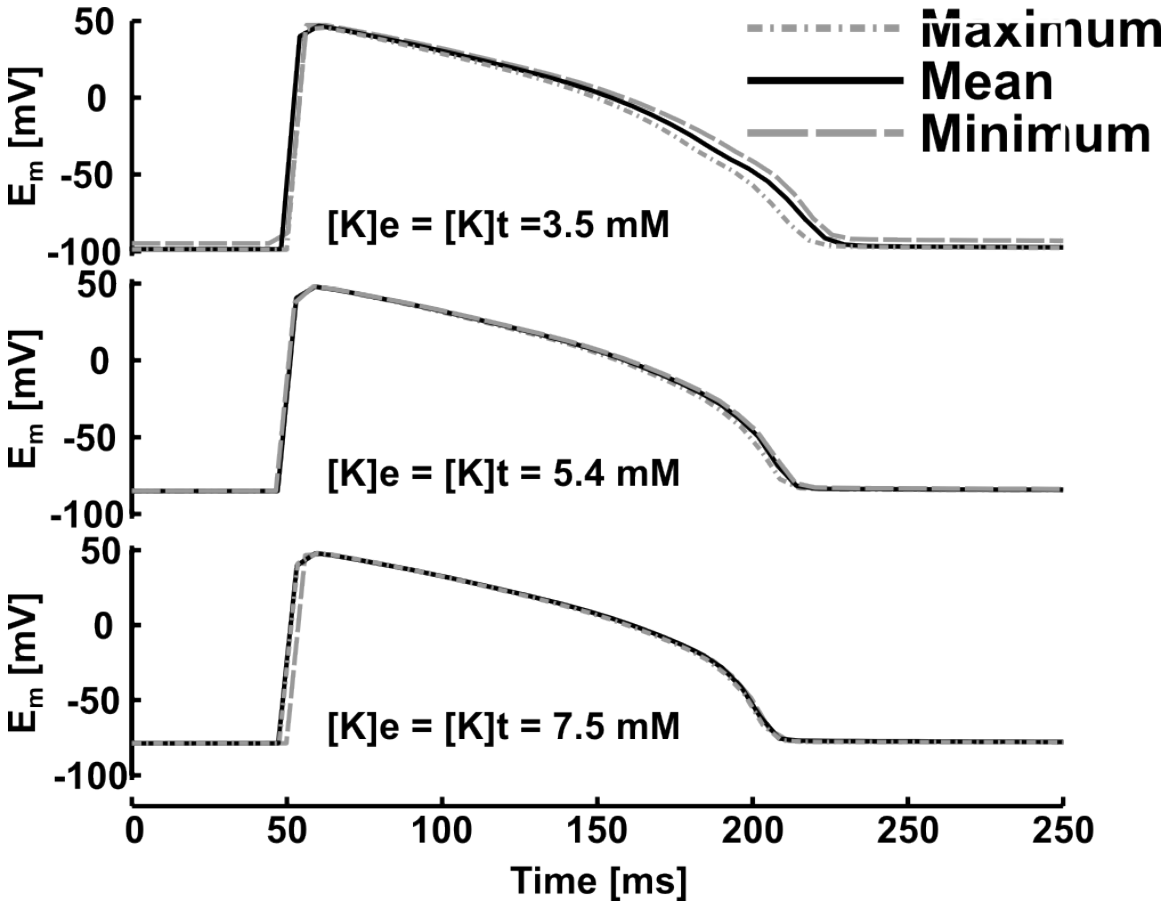

Figure 3.8: Effects of extracellular K^+-concentration on action potential shape at different t-tubular densities

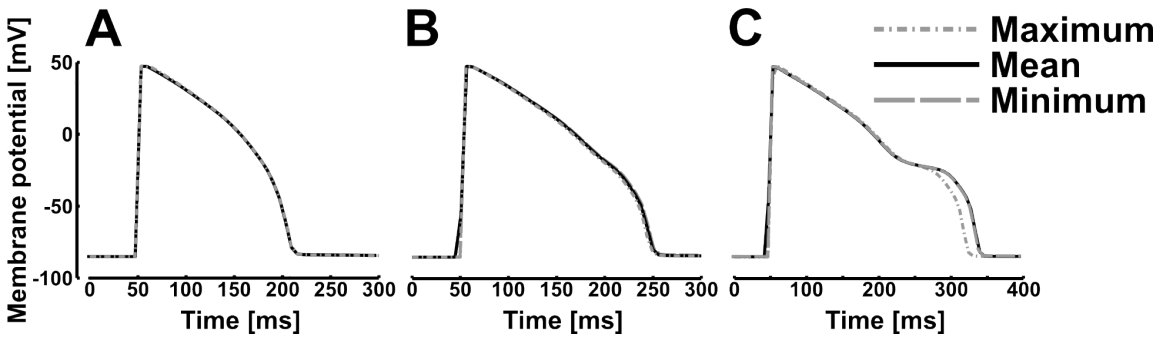

Figure 3.9: Inhibition of K^+-currents. A: uniform action potential waveform with intact K^+-currents, B: uniformly prolonged action potential waveform with complete I_{Kr}-inhibition, C: earlier repolarisation in maximally tubulated cardiomyocytes with complete I_{Ks}-inhibition ($g_{Ks} = 0$) and I_{Kr}-reduction ($g_{Kr} - 25\%$)

with intact currents (Fig. 3.9 A). With complete I_{Kr}-inhibition which was simulated by setting g_kr to 0, the action potential was prolonged uniformly in minimally, normally and maximally tubulated cardiomyocytes (Fig. 3.9 B). Complete I_{Ks}-inhibition ($g_{Ks} = 0$) combined with I_{Kr}-reduction ($g_{Kr} - 25\%$ prolonged the action potential uniformly in minimally and normally tubulated cardiomyocytes and slightly less in maximally tubulated cardiomyocytes (Fig. 3.9 C).

Chapter 4

Discussion

4.1 Generation of three-dimensional models of the t-tubular structure

In this study, three-dimensional models of the t-tubular architecture could be generated based on optical signals. This has been achieved before using multiphoton [96] and confocal microscopy [86, 66]. However, an optical approach to structural modelling of the t-tubular system is problematic as diameters of t-tubules are partially below the resolution of light. Details that contribute to the surface of the t-tubular membrane, e. g. foldings, are not to be resolved by light microscopy. Besides this general consideration, a magnitude of problems may arise at different steps in the experimental and computational workflow starting with the cell isolation. In the following section, these problems will be discussed in greater detail.

T-tubules undergo extensive remodelling after cell isolation [78]. Changes of the t-tubular structure may arise from differences in the cell isolation protocols as well as from the substances as batch-dependent differences in enzyme composition are a well known issue to the experimentalist.

An interrelated problem is the dependence of the reconstruction on the dye used for imaging. While Savio-Galimberti *et al.* [86] found a good correlation of WGA-Alexa 555 and dextran-fluorescein (molecular mass 10 kDa) in rabbit cardiomyocytes and Soeller *et al.* [96] could reconstruct the t-tubular structure based on a dextran-fluorescein at 70 kDa in rat cardiomyocytes which have t-tubules with smaller diameters, dextran-fluorescein (70 and 10 kDa) could not be dectected inside the t-tubular system at all in our study. Besides the size of the molecules, the electrical interaction between the negatively charged dextran-conjugates and the glycocalix might influence the diffusion as well as the molecular size. The enzymatic dissociation as well as

species differences might alter the composition of the t-tubular glycocalix and thus may determine failure or success of negatively charged dyes. It is, however, impossible to conclude on the relevant causes that lead to the failure of dextran-conjugates in our experiments as the composition of t-tubular matrix as well as the influence of cell isolation on the t-tubular structure are unknown. With the aforesaid, it cannot be ruled out in addition that different parts of the t-tubular system are not amenable to extracellular dyes while others are depending on their specific diameters and glycocalix composition.

Further complications arise from the imaging approach. As already mentioned, a considerable fraction of the t-tubular system has diameters too small to be resolved with optical methods. With the Rayleigh criterion $d = \frac{1.22 \cdot \lambda}{2 \cdot \mathrm{NA}}$ where λ is light wavelength and NA the numerical aperture, in our approach ($\lambda = 565$nm and NA $= 1.4$), a maximal resolution of 0.24 μm can be achieved. T-tubular diameters range from 40 to 450 nm with more than 50% between 180 and 280 nm [19]. Thus, assuming a normal distribution, half of the t-tubules are missed. The deconvolution approach compensates partially for this problem, it is however clear that even if dye penetration was perfect, a considerable fraction of the t-tubular system would be missed.

Image processing and segmentation further influences the structural modelling. The threshold-based segmentation that, in our study was used to generate a presgmentation matrix, hinges on the selection of an appropriate threshold. While it was our aim to undersegment the t-tubular system in order to use it as a seeding matrix for further region growing, selection of a threshold that is appropriate for the actual segmentation is highly arbitrary. The region growing algorithm on the other hand is dependent on parameter selection as well.

In contrast, electron tomography resolves subcellular details at – in our case – ≈ 4 nm resolution in three dimenensions. The detectable surface structure is, however, dependent on the fixation protocol. After chemical fixation, membranes were corrugated and showed small leaks. Besides the structural inaccuracy, corrugation as well as leaks interfere with manual segmentation as accurate tracing is not possible. Automatic segmentation might as well be hindered. Region-growth based algorithms could fail to stay within the membrane borders because of membrane leaks. Corrugation might interfere with adaequate edge detection. Both corrugation and leaks were not observed after high pressure freezing and subsequent high pressure freezing. Although the t-tubular structure was resolved excellently, the inner mitochondrial membrane was weakly contrasted and a sarcoplasmic reticulum could not be detected at all. To give account on these details, further protocol optimisation will be required.

The major limitation of electron tomography is the small size of the acquired volumes. This can be overcome by volume combination techniques. Here, a $2 \cdot 1$ montage was generated by combination of two volumes. In theory, montaging can be extended to the level of a whole cell. This is, however, currently mainly limited by the high time requirements.
A second limitation is the requirement of fixed preparations. While with confocal microscopy, t-tubular structure can be investigated in living cells, changes of t-tubular structure can be investigated as a function of time in one and the same preparation at a single region of interest.

4.2 Estimation of the heterogeneity of the t-tubular system based on confocal microscopy

While species differences in the size of the t-tubular system have been extensively quantified [12], differences within the ventricular wall are not well studied. However, quantification of the t-tubular system was mainly based on electron microscopy (see 1.1.3). Using confocal microsopy, regions of interest outside of the nuclear and perinuclear region were analysed. A considerable variability of t-tubular density was found between cells, while within individual cells the variability was relatively small.
Unlike the three-dimensional reconstruction, the quantification of the t-tubular variability relied on a threshold-based segmentation of small regions of interest. The underlying regions of interest, however, were small and very homogeneous with regard to fluorescence intensity. In addition, most of the data were taken from the center of cardiomyocytes where the incidence of non-specific fluorescence sources was low compared to regions adjacent to the sarcolemma.
The data do not allow any conclusion on the source of the variability as cardiomyocytes were isolated 'in bulk' from the entire ventricular tissue without any control of source localisation. As t-tubular variability could enhance repolarisation dispersion under pharmacological modulation, this could contribute to established gradients of electrophysiological function, e. g. transmural dispersion of repolarisation and thus tubulation patterns could be distributed accordingly. The regionalisation of t-tubular variability remains to be established.

4.3 Modelling the effects of t-tubular heterogeneity on electrophysiological function

A t-tubular compartment has recently been introduced into a functional model of a rabbit ventricular cardiomyocyte [77]. While the effects of changes of coupling between the surface and the t-tubular membrane and of the ion concentration in the t-tubular lumen have been investigated in great detail, the effects of changes of t-tubular dimenstions are unknown. As we observed a variability of t-tubular density within ventricular cardiomyocytes and the ion channel composition differ between t-tubular and surface membrane, we hypothesised that changes in the t-tubular density might lead to changes of the electrophysiological behaviour and might therefore contribute to heterogeneity of repolarisation. With regard to the hypothesis that there might be a connection between architecture of the t-tubular system and repolarisation, the identification of a caveolin-3 mutation as a cause of long QT syndrome is particularly interesting [108]. Caveolin-3 is involved in the formation [75] and disruption [28] of t-tubular structure. The caveolin-3-mutation underlying long QT syndrome leads primarily to a gain-of-function of the Na^+-Ca^{2+}-exchanger [108]. It is however unclear whether the t-tubular membrane structure, the distribution of the Na^+-Ca^{2+}-exchanger or the interaction between Na^+-Ca^{2+}-exchanger and caveolin-3 or the combination is the cause of the gain-of-function.
The effect of t-tubular density was simulated in the model by Pásek *et al.* [77] by changing the parameter ρ_M that describes the density of t-tubular openings in the surface membrane and correlates with the surface area of the t-tubular system according to the 25^{th}, 75^{th} percentile, the minimum and the maximum of the empirically determined t-tubular fraction.

T-tubular variability does not affect the action potential waveform under standard model conditions, but ion concentration, Ca^{2+}-cycling and ionic currents. As the t-tubular system concentrates the L-type calcium current (see 1.2.2), the inward current $I_{Ca,L}$ decreased as expected with a smaller and increased with a larger t-tubular fraction. If this would occur isolated, a prolongation of the action potential would have to be expected with a higher t-tubular density. This effect is counteracted by the increase in K^+-currents. As those were – in the model underlying the simulations – equally distributed between surface and t-tubular membrane, the current density did not change with an altered t-tubular density. The L-type Ca^{2+}-current had a 1.6x higher density in the t-tubular membrane, thus the

current density increased with the t-tubular surface area and thus with the t-tubular density ρ_M. While complete detubulation lead to a shortening of the action potential [77], the empirically determined distribution of t-tubular density did not substantial effect on the action potential duration.
Intracellular ion concentrations and Ca^{2+}-cycling between the sarcoplasmic reticulum and the intracellular space were however substantially affected by changes of the t-tubular density. The ratio between the cytosolic and subspace Ca^{2+}-concentration decreased with a higher t-tubular density. This relationship could be interpreted to reflect the experimental finding that a loss of t-tubuli leads a diffuse Ca^{2+}-release [47, 17]. The model however assumes that ion concentrations are homogeneous within the intracellular space and do not show a gradient as experimentally oberved. Thus, under standard model conditions, changes of ionic currents, ion concentrations, Ca^{2+}-handling are – within the physiological range of t-tubular variability – balanced with regard to action potential duration.

Simulated Na^+-K^+-ATPase inhibition, low K^+-concentration and inhibition of repolarisation reserve unmask electrophysiological differences depending on t-tubular density. We next tried to stress this balance by inhibition of the Na^+-K^+-ATPase and K^+-currents. Na^+-K^+-ATPase inhibition is one of the many actions of digitalis glycosides and endogenous digitalis-like hormones on the heart. The electrophysiological effects of the main action of digitalis – inhibition of the Na^+-K^+-ATPase – were extensively studied in the 70ś and 80ś. The interest into the complex action decreased before the concept of transmural dispersion of repolarisation was introduced. Taking additionally into account that digitalis lost its role as the protagonist of heart failure therapy, it is not suprising that the effect of digitalis on transmural dispersion of repolarisation is not understood. Nevertheless, digitalis has a substantial pro-arrhythmic potential and can give rise to a variety ventricular (and non-ventricular) arrhythmias. Already at a therapeutic dose, it affects the repolarisation in the electrocardiogram by shortening of the QT-interval and downslope ST-segment depression. Normally, the ST-segment in the electrocardiogram is isoelectric. However, a repolarisation gradient can change the level and the shape of the ST-segment. At the cellular level, shortening of the action potential corresponds to the shorter QT-interval. Although it is not known whether it differentially affects action potential duration in epicardial, endocardial and M cells, the ST-segment depression is highly suggestive of a gradient during the plateau phase that requires a dispersion of repolarisation. Further indication towards a differential

effect on repolarisation is the observation that the digitalis glycoside strophantidin induces afterdepolarisation mainly in M cells [92] and a transmural gradient of Na^+-K^+-activity [40]. It is therefore justified to ask wheter digitalis – albeit shortening the action potential – may enhance dispersion of repolarisation.

The modelling approach presented here was based on the reduction of the maximal I_{NKA} only and lead to a shortening of the action potential. While differences in the tubular density did not affect action potential duration with intact I_{NKA}, the shortening of the action potential was further accentuated at a higher and less pronounced at a lower tubular density. This seems to indicate that I_{NKA}-inhibtion abolishes a compensatory behaviour of the model that – despite differences in Ca^+-handling, ionic currents and ion concentration at different tubular densities – maintains the action potential duration.

A similar observation was made when the extracellular and tubular K^+-concentration was modified. Only the decrease of the K^+-concentration lead to differences of action potential duration depending on the tubular density. A partial explanation of this phaenomenon is that the activity of I_{NKA} is impeded by low extracellular K^+-concentration. In contrast to the isolated I_{NKA}-inhibition, the dispersion could also be induced at a prolonged action potential.

While the direct contribution of the Na^+-K^+-ATPase to repolarisation is small under normal intracellular Na^+-concentrations, we hypothesised that direct inhibition of repolarising currents might lead to a differential behaviour depending on the t-tubular density. The rapid component of the delayed recitfier is a major contributor to the late phase of repolarisation in ventricular cells and its inhibition was modelled by a 25% reduction of the current's conductance g_{Kr}. As exprected, a prolongation of the action potential was observed, however there were no differences depending on t-tubular density. The combination of I_{Kr}-block with complete inhibition of the slow component of the delayed rectifier, I_{Ks}, further prolonged the action potential and with a stronger prolongation in less tubulated cell, a differential behaviour was observed. *Prima facie* the block of multiple repolarising currents does not seem to be of high relevance. However, exactly this is reflected in the concept of repolarisation reserve [80]. Repolarisation reserve can be vaguely defined as "the idea is that the complexity of repolarization includes some redundancy" [81], however as it is still "a moving target" [81] it withstands a precise mechanistic defintion. Based on the observation that a loss-of-function mutation of a single repolarising current, e.g. I_{Kr}, elicits a marked QT-prolongation in some individuals while in others with the same mutation a normal QT-interval is found, it was argued that other repolarising currents can

compensate for the loss of this single currents. An example is the contribution of I_{Ks} to repolarisation which under normal conditions is small in many species. I_{Ks}-block does neither lead to a significant action potential prolongation nor to a substantial increase in other repolarising currents. If, however, I_{Kr} is inhibited, I_{Ks} increases substantially. A further I_{Ks}-block leads to a massive prolongation of the action potential. It can thus be argued that I_{Ks} is redundant under normal conditions, yet it can compensate for the loss of currents that contribute to repolarisation [107]. Repolarisation reserve is indeed reflected in other models of the ventricular cardiomyocyte as investigated by Fink *et al.* [36]. With the idea that a repolarisation reserve-like mechanism can attenuate a different reponse to inhibition of K^+-currents depending on t-tubular density, the effects of a combined current reduction were investigated.

Limitations of the modelling approach. Care has to be taken when conclusions are drawn from this approach. The assumption that channel distribution varies independently from variations in the t-tubular system is not based on any studies. To the contrary, in diseases that are associated with t-tubular remodelling, a redistribution of ionic channels was observed. Whether the distribution of ionic channels varies with the surface area of t-tubules is not known. Furthermore, although the work by Pásek *et al.* is pioneering by integrating t-tubules into a ventricular cardiomyocyte model, the variability of t-tubules within the cell is not taken into account. However, it is likely that the complexity of the three-dimensional structure of the t-tubular system (see 1.1.3 and 3.2) – if implemented into a model – might reveal yet more complex behaviour of patho-physiological relevance. It can be hypothesised that redundancy of the t-tubular system exist within in cells that extends beyond density of the t-tubular membrane. This might be used to reduce complexity of anatomical models in order to ease implementation of functional parameters.

4.4 Conclusion and outlook

The computational modelling data support the notion that alterations and variability of the t-tubular structure may lead to altered electrophysiological behaviour without requiring a redistribution of ion channels. The representation of the t-tubular system in electrophysiological models of cardiomyocytes is, however, still greatly simplified as it is based on a lumped 'pseudo-two-dimensional' representation, instead of a three-dimensional model. Three-dimensional reconstructions of the t-tubular system are

possible using light microscopy and might approximate the t-tubular structure better than a cylindric compartment. This, as a major fraction of the t-tubular cannot be resolved by conventional confocal microscopy, remains however to be verified by higher-resolution techniques. Electron tomography could provide an adequate resolution in three dimensions. Although imaging of living cells is not possible, high pressure freezing and subsequent freeze substitution could provide a better structural preservation than chemical fixation. The second major disadvantage, the relatively small volumes of single tomograms, could be overcome by volume combination techniques. An alternative approach could be based on block-face imaging of the cell surfaces cut by focussed ion beam approaches, which will give mesoscopic data for entire cells with image voxel dimensions of 110-120 nm.

Chapter 5

Acknowledgements

I wish to express my warmest gratitude to Prof Peter Kohl for supervision and support in the last year as well as to Dr Vicente Grau and to Prof Len Seymour who provided me with advise and supervision.
Many thanks to Prof Andy Hoenger, Mary Morphew and Eileen O'Toole, University of Colorado at Boulder for the great introduction into electron tomography, data acquisition and data analysis. I wish to thank Dr Christian Bollensdorff for a lot of support. Philipp Cobden, Department of Physiology, Anatomy and Genetics as well as Andy Edwards, now University of California San Diego, generously provided me with cardiomyocytes.
I am grateful for the support of the Medical Research Council.

References

[1] S. P. H. Alexander, A. Mathie, and J. A. Peters. Ion channels. *British Journal of Pharmacology*, 150 Suppl 1:96, 2007.

[2] W. Almers. Potassium conductance changes in skeletal muscle and the potassium concentration in the transverse tubules. *Journal of Physiology*, 225:33–56, 1972.

[3] W. Almers. Potassium concentration changes in the transverse tubules of vertebrate skeletal muscle. *Federation Proceedings*, 39:1527–1532, 1980.

[4] J. Amsellem, R. Delorme, C. Souchier, and C. Ojeda. Transverse-axial tubular system in guinea pig ventricular cardiomyocyte: 3D reconstruction, quantification and its possible role in K^+ accumulation-depletion phenomenon in single cells. *Biology of the Cell*, 85:43–54, 1995.

[5] C. Antzelevitch. Cellular basis for the repolarization waves of the ECG. *Annals of the New York Academy of Sciences*, 1080:268–281, 2006.

[6] C. Antzelevitch. Ionic, molecular, and cellular bases of QT-interval prolongation and torsade de pointes. *Europace*, 9 Suppl 4:iv4–i15, 2007.

[7] C. Antzelevitch. Drug-induced spatial dispersion of repolarization. *Cardiology Journal*, 15:100–121, 2008.

[8] E. P. Anyukhovsky, E. A. Sosunov, R. Z. Gainullin, and M. R. Rosen. The controversial M cell. *Journal of Cardiovascular Electrophysiology*, 10:244–260, 1999.

[9] P. Asghari, M. Schulson, D. R. L. Scriven, G. Martens, and Edwin D. W. Moore. Axial tubules of rat ventricular myocytes form multiple junctions with the sarcoplasmic reticulum. *Biophysical Journal*, 96:4651–4660, 2009.

[10] A. S. Ayettey and V. Navaratnam. The t-tubule system in the specialized and general myocardium of the rat. *Journal of Anatomy*, 127:125–140, 1978.

[11] R. G. Berry, S. Despa, W. Fuller, D. M. Bers, and M. J. Shattock. Differential distribution and regulation of mouse cardiac Na^+/ K^+-ATPase α_1 and α_2 subunits in t-tubule and surface sarcolemmal membranes. *Cardiovascular Research*, 73:92–100, 2007.

[12] D. Bers. *Excitation-Contraction Coupling and Cardiac Contractile Force*. Elsevier, 2nd ed. edition, 2001.

[13] L. A. Blatter and E. Niggli. Confocal near-membrane detection of calcium in cardiac myocytes. *Cell Calcium*, 23:269–279, 1998.

[14] M. D. Bootman, D. R. Higazi, S. Coombes, and H. L. Roderick. Calcium signalling during excitation-contraction coupling in mammalian atrial myocytes. *Journal of Cell Science*, 119:3915–3925, 2006.

[15] R. Bouchard, R. B. Clark, A. E. Juhasz, and W. R. Giles. Changes in extracellular K^+ concentration modulate contractility of rat and rabbit cardiac myocytes via the inward rectifier K^+ current IK1. *Journal of Physiology*, 556:773–790, 2004.

[16] N. Brandt. Identification of two populations of cardiac microsomes with nitrendipine receptors: correlation of the distribution of dihydropyridine receptors with organelle specific markers. *Archives of Biochemistry and Biophysics*, 242:306–319, 1985.

[17] F. Brette, S. Despa, D. M. Bers, and C. H. Orchard. Spatiotemporal characteristics of SR Ca^{2+} uptake and release in detubulated rat ventricular myocytes. *Journal of Molecular and Cellular Cardiology*, 39:804–812, 2005.

[18] F. Brette, K. Komukai, and C. H. Orchard. Validation of formamide as a detubulation agent in isolated rat cardiac cells. *American Journal of Physiology. Heart and Circulatory Physiology*, 283:H1720–H1728, 2002.

[19] F. Brette and C. Orchard. T-tubule function in mammalian cardiac myocytes. *Circulation Research*, 92:1182–1192, 2003.

[20] F. Brette, L. Sallé, and C. H. Orchard. Differential modulation of L-type Ca^{2+} current by SR Ca^{2+} release at the t-tubules and surface membrane of rat ventricular myocytes. *Circulation Research*, 95:e1–e7, Jul 2004.

[21] F. Brette, L. Sallé, and C. H. Orchard. Quantification of calcium entry at the t-tubules and surface membrane in rat ventricular myocytes. *Biophysical Journal*, 90:381–389, 2006.

[22] R. Brugada, J. Brugada, C. Antzelevitch, G. E. Kirsch, D. Potenza, J. A. Towbin, and P. Brugada. Sodium channel blockers identify risk for sudden death in patients with st-segment elevation and right bundle branch block but structurally normal hearts. *Circulation*, 101:510, 2000.

[23] G. Bu, H. Adams, E. J. Berbari, and M. Rubart. Uniform action potential repolarization within the sarcolemma of in situ ventricular cardiomyocytes. *Biophysical Journal*, 96:2532–2546, 2009.

[24] E. J. Cartwright, K. Schuh, and L. Neyses. Calcium transport in cardiovascular health and disease – the sarcolemmal calcium pump enters the stage. *Journal of Molecular and Cellular Cardiology*, 39:403–406, 2005.

[25] A. Chase and C. H. Orchard. Ca^{2+} efflux via the sarcolemmal Ca^{2+} ATPase occurs only in the t-tubules of rat ventricular myocytes. *Journal of Molecular and Cellular Cardiology*, 50:187–193, 2011.

[26] L. Cleemann and M. Morad. Extracellular potassium accumulation and inward-going potassium rectification in voltage clamped ventricular muscle. *Science*, 191(4222):90–92, 1976.

[27] L. Cleemann and M. Morad. Extracellular potassium accumulation in voltage-clamped frog ventricular muscle. *Journal of Physiology*, 286:83–111, 1979.

[28] D. J. Crossman, P. N. Ruygrok, P. R. Ruygrok, C. Soeller, and M. B. Cannell. Changes in the organization of excitation-contraction coupling structures in failing human heart. *PLoS ONE*, 6:e17901, 2011.

[29] S. Despa, F. Brette, C. H. Orchard, and D. M. Bers. Na/Ca exchange and Na/K-ATPase function are equally concentrated in transverse tubules of rat ventricular myocytes. *Biophysical Journal*, 85:3388–3396, 2003.

[30] S. Dhein. Pharmacology of gap junctions in the cardiovascular system. *Cardiovascular Research*, 62:287–298, 2004.

[31] K. M. Dibb, J. D. Clarke, M. A. Horn, M. A. Richards, H. K. Graham, D. A. Eisner, and A. W. Trafford. Characterization of an extensive transverse tubular network in sheep atrial myocytes and its depletion in heart failure. *Circulation. Heart Failure*, 2:482–489, 2009.

[32] John R. Dietz. Mechanisms of atrial natriuretic peptide secretion from the atrium. *Cardiovascular Research*, 68:8–17, 2005.

[33] D. D. Doyle, T. J. Kamp, H. C. Palfrey, R. J. Miller, and E. Page. Separation of cardiac plasmalemma into cell surface and t-tubular components. distribution of saxitoxin- and nitrendipine-binding sites. *The Journal of Biological Chemistry*, 261:6556–6563, 1986.

[34] V. Dyachenko, B. Husse, U. Rueckschloss, and G. Isenberg. Mechanical deformation of ventricular myocytes modulates both TRPC6 and Kir2.3 channels. *Cell Calcium*, 45:38–54, 2009.

[35] A. Fabiato. Calcium-induced release of calcium from the cardiac sarcoplasmic reticulum. *The American Journal of Physiology*, 245:C1–14, 1983.

[36] M. Fink, W. R. Giles, and D. Noble. Contributions of inwardly rectifying K^+ currents to repolarization assessed using mathematical models of human ventricular myocytes. *Philosophical Transactions. Series A*, 364(1842):1207–1222, 2006.

[37] A. Fleckenstein, J. Janke, H. J. Döring, and O. Leder. Myocardial fiber necrosis due to intracellular Ca overload – a new principle in cardiac pathophysiology. *Recent advances in Studies on Cardiac Structure and Metabolism*, 4:563–580, 1974.

[38] J. K. Foskett, C. White, K. Cheung, and D. D. Mak. Inositol trisphosphate receptor Ca^{2+} release channels. *Physiological Reviews*, 87:593–658, 2007.

[39] C. Franzini-Armstrong. Simultaneous maturation of transverse tubules and sarcoplasmic reticulum during muscle differentiation in the mouse. *Developmental Biology*, 146:353–363, 1991.

[40] J. Gao, W. Wang, I. S. Cohen, and R. T. Mathias. Transmural gradients in Na/K pump activity and $[Na^+]_i$ in canine ventricle. *Biophysical Journal*, 89:1700–1709, 2005.

[41] A. V. Glukhov, V. V. Fedorov, Q. Lou, V. K. Ravikumar, P. W. Kalish, R. B. Schuessler, N. Moazami, and I. R. Efimov. Transmural dispersion of repolarization in failing and nonfailing human ventricle. *Circulation Research*, 106:981–991, 2010.

[42] T. Gotoh. Quantitative studies on the ultrastructural differentiation and growth of mammalian cardiac muscle cells. the atria and ventricles of the cat. *Acta Anatomica*, 115:168–177, 1983.

[43] F. Guharay and F. Sachs. Stretch-activated single ion channel currents in tissue-cultured embryonic chick skeletal muscle. *Journal of Physiology*, 352:685–701, 1984.

[44] I. Gussak, N. Liebl, S. Nouri, P. Bjerregaard, F. Zimmerman, and B. R. Chaitman. Deceleration-dependent shortening of the QT interval: a new electrocardiographic phenomenon? *Clinical Cardiology*, 22:124–126, 1999.

[45] J. Han and G. K. Moe. Nonuniform recovery of excitability in ventricular muscle. *Circulation Research*, 14:44–60, 1964.

[46] C. Hauck, T. Potter, M. Bartz, T. Wittwer, T. Wahlers, U. Mehlhorn, G. Scheiner-Bobis, A. A. McDonough, W. Bloch, R. H. G. Schwinger, and J. Müller-Ehmsen. Isoform specificity of cardiac glycosides binding to human Na^+, K^+-ATPase $\alpha_1\beta_1$, $\alpha_2\beta_1$ and $\alpha_3\beta_1$. *European Journal of Pharmacology*, 622:7–14, 2009.

[47] J. Hüser, S. L. Lipsius, and L. A. Blatter. Calcium gradients during excitation-contraction coupling in cat atrial myocytes. *Journal of Physiology*, 494:641–651, 1996.

[48] M. Ibrahim, J. Gorelik, M. H. Yacoub, and C. M. Terracciano. The structure and function of cardiac t-tubules in health and disease. *Proceedings of the Royal Society. Series B*, 278:2714–2723, 2011.

[49] P. F. James, I. L. Grupp, G. Grupp, A. L. Woo, G. R. Askew, M. L. Croyle, R. A. Walsh, and J. B. Lingrel. Identification of a specific role for the Na,K-ATPase α_2 isoform as a regulator of calcium in the heart. *Molecular Cell*, 3:555–563, 1999.

[50] E. Janowski, L. Cleemann, P. Sasse, and M. Morad. Diversity of Ca^{2+} signaling in developing cardiac cells. *Annals of the New York Academy of Sciences*, 1080:154–164, 2006.

[51] M. M. Kirk, L. T. Izu, Ye Chen-Izu, S. L. McCulle, W. G. Wier, C. W. Balke, and S. R. Shorofsky. Role of the transverse-axial tubule system in generating calcium sparks and calcium transients in rat atrial myocytes. *Journal of Physiology*, 547:441–451, 2003.

[52] R. Kline and M. Morad. Potassium efflux and accumulation in heart muscle. evidence from K +/- electrode experiments. *Biophysical Journal*, 16:367–372, 1976.

[53] R. P. Kline and M. Morad. Potassium efflux in heart muscle during activity: extracellular accumulation and its implications. *Journal of Physiology*, 280:537–558, 1978.

[54] P. Kohl, P. J. Cooper, and H. Holloway. Effects of acute ventricular volume manipulation on in situ cardiomyocyte cell membrane configuration. *Progress in Biophysics and Molecular Biology*, 82(1-3):221–227, 2003.

[55] P. Kohl, F. Sachs, and M. R. Franz. *Cardiac mechano-electric feedback and arrhythmias: from pipette to patient.* Elsevier, 2005.

[56] K. Komukai, F. Brette, T. T. Yamanushi, and C. H. Orchard. K^+ current distribution in rat sub-epicardial ventricular myocytes. *Pflügers Archiv : European Journal of Physiology*, 444:532–538, 2002.

[57] Y. E. Korchev, M. Raval, M. J. Lab, J. Gorelik, C. R. Edwards, T. Rayment, and D. Klenerman. Hybrid scanning ion conductance and scanning near-field optical microscopy for the study of living cells. *Biophysical Journal*, 78:2675–2679, 2000.

[58] A. J. Levi, M. R. Boyett, and C. O. Lee. The cellular actions of digitalis glycosides on the heart. *Progress in Biophysics and Molecular Biology*, 62:1–54, 1994.

[59] G. R. Li, J. Feng, L. Yue, and M. Carrier. Transmural heterogeneity of action potentials and I_{to1} in myocytes isolated from the human right ventricle. *The American Journal of Physiology*, 275:H369–H377, 1998.

[60] G. Lim, L. Venetucci, D. A. Eisner, and B. Casadei. Does nitric oxide modulate cardiac ryanodine receptor function? implications for excitation-contraction coupling. *Cardiovascular Research*, 77:256–264, 2008.

[61] E. Lindner. Die submikroskopische Morphologie des Herzmuskels. *Cell and Tissue Research*, 45:702–746, 1957.

[62] D. W. Liu and C. Antzelevitch. Characteristics of the delayed rectifier current (IKr and IKs) in canine ventricular epicardial, midmyocardial, and endocardial myocytes. a weaker IKs contributes to the longer action potential of the M cell. *Circulation Research*, 76:351–365, 1995.

[63] W. E. Louch, H. K. Mørk, J. Sexton, T. A. Strømme, P. Laake, I. Sjaastad, and O. M. Sejersted. T-tubule disorganization and reduced synchrony of Ca^{2+} release in murine cardiomyocytes following myocardial infarction. *Journal of Physiology*, 574:519–533, 2006.

[64] A. R. Lyon, K. T. MacLeod, Y. Zhang, E. Garcia, G. K. Kanda, M. J. Lab, Y. E. Korchev, S. E. Harding, and J. Gorelik. Loss of t-tubules and other changes to surface topography in ventricular myocytes from failing human and rat heart. *Proceedings of the National Academy of Sciences of the United States of America*, 106(16):6854–6859, 2009.

[65] G. Martin and M. Morad. Activity-induced potassium accumulation and its uptake in frog ventricular muscle. *Journal of Physiology*, 328:205–227, Jul 1982.

[66] T. G. McNary, J. H. B. Bridge, and F. B. Sachse. Strain transfer in ventricular cardiomyocytes to their transverse tubular system revealed by scanning confocal microscopy. *Biophysical Journal*, 100:L53–L55, 2011.

[67] B. Mellström, M. Savignac, R. Gomez-Villafuertes, and Jose R. Naranjo. Ca^{2+}-operated transcriptional networks: molecular mechanisms and in vivo models. *Physiological Reviews*, 88:421–449, 2008.

[68] P. J. Mohler, J. Q. Davis, and V. Bennett. Ankyrin-B coordinates the Na/K ATPase, Na/Ca exchanger, and InsP3 receptor in a cardiac T-tubule/SR microdomain. *PLoS Biology*, 3:e423, 2005.

[69] P. J. Mohler, J. J. Schott, A. O. Gramolini, K. W. Dilly, S. Guatimosim, W. H. duBell, L. Song, K. Haurogné, F. Kyndt, Mervat E. Ali, Terry B. Rogers, W. J. Lederer, D. Escande, H. Le Marec, and V. Bennett. Ankyrin-B mutation causes type 4 long-QT cardiac arrhythmia and sudden cardiac death. *Nature*, 421:634–639, 2003.

[70] P. J. Mohler, Igor Splawski, C. Napolitano, G. Bottelli, L. Sharpe, K. Timothy, S. G. Priori, M. T. Keating, and V. Bennett. A cardiac arrhythmia syndrome caused by loss of ankyrin-B function. *Proceedings of the National Academy of Sciences of the United States of America*, 101:9137–9142, 2004.

[71] M. Morad. Physiological implications of K^+ accumulation in heart muscle. *Federation Proceedings*, 39:1533–1539, 1980.

[72] S. Nattel, C. Antzelevitch, and D. Noble. Resolving the M-cell debate: why and how. *Heart Rhythm*, 8:1293–1295, 2011.

[73] J. O-Uchi, H. Sasaki, S. Morimoto, Y. Kusakari, H. Shinji, T. Obata, K. Hongo, K. Komukai, and S. Kurihara. Interaction of α_1-adrenoceptor subtypes with different G proteins induces opposite effects on cardiac L-type Ca^{2+} channel. *Circulation Research*, 102:1378–1388, 2008.

[74] C. H. Orchard, M. Pásek, and F. Brette. The role of mammalian cardiac t-tubules in excitation-contraction coupling: experimental and computational approaches. *Experimental Physiology*, 94:509–519, 2009.

[75] R. G. Parton, M. Way, N. Zorzi, and E. Stang. Caveolin-3 associates with developing t-tubules during muscle differentiation. *The Journal of Cell Biology*, 136:137–154, 1997.

[76] M. Pásek, F. Brette, A. Nelson, C. Pearce, A. Qaiser, G. Christe, and C. H. Orchard. Quantification of t-tubule area and protein distribution in rat cardiac ventricular myocytes. *Progress in Biophysics and Molecular Biology*, 96:244–257, 2008.

[77] M. Pásek, J. Simurda, C. H. Orchard, and Georges Christé. A model of the guinea-pig ventricular cardiac myocyte incorporating a transverse-axial tubular system. *Progress in Biophysics and Molecular Biology*, 96(1-3):258–280, 2008.

[78] D. Pavlović, L. M. McLatchie, and M. J. Shattock. The rate of loss of t-tubules in cultured adult ventricular myocytes is species dependent. *Experimental Physiology*, 95:518–527, 2010.

[79] D. G. Rayns, F. O. Simpson, and W. S. Bertaud. Transverse tubule apertures in mammalian myocardial cells: surface array. *Science*, 156(3775):656–657, 1967.

[80] D. M. Roden. Taking the idio out of idiosyncratic: predicting torsades de pointes. *Pacing and Clinical Electrophysiology : PACE*, 21:1029–1034, 1998.

[81] D. M. Roden. Repolarization reserve: a moving target. *Circulation*, 118(10):981–982, 2008.

[82] A. Rodríguez-Sinovas, J. Cinca, A. Tapias, L. Armadans, M. Tresànchez, and J. Soler-Soler. Lack of evidence of M-cells in porcine left ventricular myocardium. *Cardiovascular Research*, 33:307–313, 1997.

[83] R. Rubio and N. Sperelakis. Entrance of colloidal ThO_2 tracer into the t tubules and longitudinal tubules of the guinea pig heart. *Zeitschrift für Zellforschung und mikroskopische Anatomie*, 116:20–36, 1971.

[84] L. Sallé, S. Kharche, H. Zhang, and F. Brette. Mechanisms underlying adaptation of action potential duration by pacing rate in rat myocytes. *Progress in Biophysics and Molecular Biology*, 96:305–320, 2008.

[85] H. Satoh, L. M. Delbridge, L. A. Blatter, and D. M. Bers. Surface: volume relationship in cardiac myocytes studied with confocal microscopy and membrane capacitance measurements species-dependence and developmental effects. *Biophysical Journal*, 70:1494–1504, 1996.

[86] E. Savio-Galimberti, J. Frank, M. Inoue, J. I. Goldhaber, M. B. Cannell, J. H. B. Bridge, and F. B. Sachse. Novel features of the rabbit transverse tubular system revealed by quantitative analysis of three-dimensional reconstructions from confocal images. *Biophysical Journal*, 95:2053–2062, 2008.

[87] P. J. Schwartz, M. Periti, and A. Malliani. The long Q-T syndrome. *American Heart Journal*, 89:378–390, 1975.

[88] S. Seki, M. Nagashima, Y. Yamada, M. Tsutsuura, T. Kobayashi, A. Namiki, and N. Tohse. Fetal and postnatal development of Ca^{2+} transients and Ca^{2+} sparks in rat cardiomyocytes. *Cardiovascular Research*, 58:535–548, 2003.

[89] C. Shen, M. J. Lin, A. Yaradanakul, V. Lariccia, J. A. Hill, and D. W. Hilgemann. Dual control of cardiac Na^+ Ca^{2+} exchange by PIP_2: analysis of the surface membrane fraction by extracellular cysteine PEGylation. *Journal of Physiology*, 582:1011–1026, 2007.

[90] N. Shepherd and H. B. McDonough. Ionic diffusion in transverse tubules of cardiac ventricular myocytes. *The American Journal of Physiology*, 275:H852–H860, 1998.

[91] S. Sicouri and C. Antzelevitch. A subpopulation of cells with unique electrophysiological properties in the deep subepicardium of the canine ventricle. the M cell. *Circulation Research*, 68:1729–1741, 1991.

[92] S. Sicouri and C. Antzelevitch. Drug-induced afterdepolarizations and triggered activity occur in a discrete subpopulation of ventricular muscle cells (M cells) in the canine heart: quinidine and digitalis. *Journal of Cardiovascular Electrophysiology*, 4:48–58, 1993.

[93] S. Sicouri, M. Quist, and C. Antzelevitch. Evidence for the presence of M cells in the guinea pig ventricle. *Journal of Cardiovascular Electrophysiology*, 7:503–511, 1996.

[94] S. Sicouri, K. W. Timothy, A. C. Zygmunt, A. Glass, R. J. Goodrow, L. Belardinelli, and C. Antzelevitch. Cellular basis for the electrocardiographic and arrhythmic manifestations of timothy syndrome: effects of ranolazine. *Heart Rhythm*, 4:638–647, 2007.

[95] I. Smyrnias, W. Mair, D. Harzheim, S. A. Walker, H. L. Roderick, and M. D. Bootman. Comparison of the t-tubule system in adult rat ventricular and atrial myocytes, and its role in excitation-contraction coupling and inotropic stimulation. *Cell Calcium*, 47:210–223, 2010.

[96] C. Soeller and M. B. Cannell. Examination of the transverse tubular system in living cardiac rat myocytes by 2-photon microscopy and digital image-processing techniques. *Circulation Research*, 84:266–275, 1999.

[97] L. S. Song, E. A. Sobie, S. McCulle, W. J. Lederer, C. W. Balke, and H. Cheng. Orphaned ryanodine receptors in the failing heart. *Proceedings of the National Academy of Sciences of the United States of America*, 103(11):4305–4310, 2006.

[98] I. Splawski, K. W. Timothy, L. M. Sharpe, N. Decher, P. Kumar, R. Bloise, C. Napolitano, P. J. Schwartz, R. M. Joseph, K. Condouris, H. Tager-Flusberg, S. G. Priori, M. C. Sanguinetti, and M. T. Keating. Ca(V)1.2 calcium channel dysfunction causes a multisystem disorder including arrhythmia and autism. *Cell*, 119:19–31, 2004.

[99] T. Stankovicova, M. Szilard, I. De Scheerder, and K. R. Sipido. M cells and transmural heterogeneity of action potential configuration in myocytes from the left ventricular wall of the pig heart. *Cardiovascular Research*, 45:952–960, 2000.

[100] F. Swift, J. A. K. Birkeland, N. Tovsrud, U. H. Enger, J. M. Aronsen, W. E. Louch, I. Sjaastad, and O. M. Sejersted. Altered Na^+/Ca^{2+}-exchanger activity due to downregulation of $Na^+/\ K^+$-ATPase α_2-isoform in heart failure. *Cardiovascular Research*, 78:71–78, 2008.

[101] Fredrik Swift, T. A. Strømme, B. Amundsen, O. M. Sejersted, and I. Sjaastad. Slow diffusion of K^+ in the t tubules of rat cardiomyocytes. *Journal of Applied Physiology*, 101:1170–1176, 2006.

[102] P. Taggart, P. Sutton, T. Opthof, R. Coronel, and P. Kallis. Electrotonic cancellation of transmural electrical gradients in the left ventricle in man. *Progress in Biophysics and Molecular Biology*, 82:243–254, 2003.

[103] P. Taggart, P. M. Sutton, T. Opthof, R. Coronel, R. Trimlett, W. Pugsley, and P. Kallis. Transmural repolarisation in the left ventricle in humans during normoxia and ischaemia. *Cardiovascular Research*, 50:454–462, 2001.

[104] Y. Takagishi, K. Yasui, N. J. Severs, and Y. Murata. Species-specific difference in distribution of voltage-gated L-type Ca^{2+} channels of cardiac myocytes. *American Journal of Physiology. Cell Physiology*, 279:C1963–C1969, 2000.

[105] S. Takeuchi, Y. Takagishi, K. Yasui, Y. Murata, J. Toyama, and I. Kodama. Voltage-gated K^+-Channel, Kv4.2, localizes predominantly to the transverse-axial tubular system of the rat myocyte. *Journal of Molecular and Cellular Cardiology*, 32:1361–1369, 2000.

[106] J. Tamargo, R. Caballero, R. Gómez, C. Valenzuela, and E. Delpón. Pharmacology of cardiac potassium channels. *Cardiovascular Research*, 62:9–33, 2004.

[107] A. Varró and I. Baczkó. Cardiac ventricular repolarization reserve: a principle for understanding drug-related proarrhythmic risk. *British Journal of Pharmacology*, 164:14–36, 2011.

[108] M. Vatta, M. J. Ackerman, B. Ye, J. C. Makielski, E. E. Ughanze, E. W. Taylor, D. J. Tester, R. C. Balijepalli, J. D. Foell, Z. Li, T. J. Kamp, and J. A. Towbin. Mutant caveolin-3 induces persistent late sodium current and is associated with long-QT syndrome. *Circulation*, 114:2104–2112, 2006.

[109] M. Wibo, G. Bravo, and T. Godfraind. Postnatal maturation of excitation-contraction coupling in rat ventricle in relation to the subcellular localization and surface density of 1,4-dihydropyridine and ryanodine receptors. *Circulation Research*, 68:662–673, 1991.

[110] J. C. Williams, A. L. Armesilla, T. M. A. Mohamed, C. L. Hagarty, F. H. McIntyre, S. Schomburg, A. O. Zaki, D. Oceandy, E. J. Cartwright, M. H. Buch, M. Emerson, and L. Neyses. The sarcolemmal calcium pump, α_1 syntrophin, and neuronal nitric-oxide synthase are parts of a macromolecular protein complex. *The Journal of Biological Chemistry*, 281:23341–23348, 2006.

[111] G. X. Yan and C. Antzelevitch. Cellular basis for the normal T wave and the electrocardiographic manifestations of the long-QT syndrome. *Circulation*, 98:1928–1936, 1998.

[112] Z. Yang, C. Pascarel, D. S. Steele, K. Komukai, F. Brette, and C. H. Orchard. Na^+-Ca^{2+} exchange activity is localized in the t-tubules of rat ventricular myocytes. *Circulation Research*, 91:315–322, 2002.

[113] Y. H. Yeh, R. Wakili, X. Y. Qi, D. Chartier, P. Boknik, S. Kääb, U. Ravens, P. Coutu, D. Dobrev, and S. Nattel. Calcium-handling abnormalities underlying atrial arrhythmogenesis and contractile dysfunction in dogs with congestive heart failure. *Circulation. Arrhythmia and Electrophysiology*, 1:93–102, 2008.

[114] T. Zeng, G. C. Bett, and F. Sachs. Stretch-activated whole cell currents in adult rat cardiac myocytes. *American Journal of Physiology. Heart and Circulatory Physiology*, 278:H548–H557, 2000.

[115] A. C. Zygmunt, G. T. Eddlestone, G. P. Thomas, V. V. Nesterenko, and C. Antzelevitch. Larger late sodium conductance in M cells contributes to

electrical heterogeneity in canine ventricle. *American Journal of Physiology. Heart and Circulatory Physiology*, 281:H689–H697, 2001.

[116] A. C. Zygmunt, R. J. Goodrow, and C. Antzelevitch. Inaca contributes to electrical heterogeneity within the canine ventricle. *American Journal of Physiology. Heart and Circulatory Physiology*, 278:H1671–H1678, 2000.